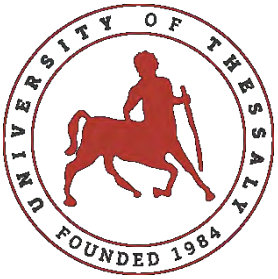

UNIVERSITY OF THESSALY
ENGINEERING SCHOOL
DEPARTMENT OF MECHANICAL ENGINEERING

Liquid Jet in Crossflow

Papakonstantinou Konstantinos

Submitted in partial fulfilment of the requirements for the Diploma of Mechanical Engineering

VOLOS, February 2019

Thesis Committee

1st Member:(Supervisor)

Assistant Prof. G. Charalampous

Department of Mechanical Engineering, University of Thessaly

2nd Member: Prof. A. Stamatelos

Department of Mechanical Engineering, University of Thessaly

3rd Member: Prof. N. Pelekasis

Department of Mechanical Engineering, University of Thessaly

Abstract

In the current work, an experimental investigation of the characteristics of a liquid jet injected into a gaseous cross flow is performed. The liquid jet was produced by an air assist atomiser while the working liquid throughout the investigation was water. The gas cross flow was air. The parameters of the investigation were the cross section average gas velocity and the liquid flow rate. The resulting Reynolds number, the aerodynamic Weber number and the gas to liquid momentum flux ratio ranges of the considered flows were Re=1349-2993, We=0.04-1.34, and $q=1x10^{-4}$–-$161x10^{-4}$. Visualisation of the liquid jet in the crossflow was conducted by shadowgraphy and an algorithm was developed to process the datasets of the experimental measurements. Special attention is given on the liquid jet trajectories and their variability. The mean liquid jet trajectories were modelled for each flow condition by power law functions. The quality of the model was quantified by the mean absolute deviation. In addition, the liquid penetration length in the stream-wise and cross-stream direction and the overall break up length were evaluated.

Acknowledgements

First of all, I would like to thank and to express my truthful gratefulness to my supervisor professor Georgios Charalampous for supporting me and guiding me during my Thesis study. His consecutive guidance advice and his knowledge were decisive for my research and the conduct of experimental process.

I would also like to thank and to express my thankfulness to my family for their continuous support during the whole period of my studies.

Table of Contents

List of Figures

List of Tables

Nomenclature

D	Droplet diameter	μm
Re	Reynolds number	-
V	Droplet volume	L3
$W_{G,L}$	Weber number	-
α	Jet radius	m
σ	Surface tension	N/m
μ	Fluid dynamic viscosity	Pa*s
p_I	Internal pressure	Pa
p_A	External aerodynamic pressure	Pa
p_σ	Surface tension pressure	Pa
C_D	Drag coefficient	-
ρ_L	Liquid density	kg/m3
ρ_A	Air density	kg/m3
U_R	Relative velocity	m/s
λ	Wavelength of disturbance	m
d	Liquid jet diameter	mm
U_0	Jet exit velocity	m/s
L	Break up length	mm
X	x coordinates	-
Y	y coordinates	-
q	Air-to-liquid momentum flux ratio	-
A_{air}	Air surface	m^2

A_{liq}	Liquid surface	m^2
u	Cross-flow velocity	m/s
D_0	Nozzle diameter	m
T	Time	sec
P	Pressure	bar
Φ	Mass flux	$kg/s*m^2$
m	Mass flow	kg/s
MR	Momentum ratio	-
Q	Flow rate	cc/min

1. Introduction

1.1 Generally

Part of the scientific field is occupied with the atomization in liquid jets and the dispersion of large and small particles and droplets into an air flow environment. This is very important in modern life, especially in industrialized procedures and domestic applications, where are required a spray form, rather than a continuous liquid jet flow. Numerous spray devices are present in gas turbine engines, spark-ignition engines, rocket engines, internal combustion engines, where use crossflow configuration for fuel injection and in several practices in other realms such as agriculture, dust control, general medicine and pharmacy. Due to the random physical form of the resultant spray during the atomization process, there is the challenge to characterize and investigate the process and the final liquid transformation included the various range of structures size. For this reason is primary importance to understand the liquid bulk break up characteristics and the process of an involving spray as well the formed structure and the development techniques. These days the combination of experimental and numerical methods are used to achieved the complicated task of developing process of breakup theory. A better understanding of the basic atomization process could improve the efficiency of combustion, reduce fuel consumption and decrease the pollutant emissions. Efforts, also, associated with the precision manufacturing of liquid injector devices and with the evolution of atomization technology.

The process of liquid mass atomization, can be described as the procedure where a liquid jet is disintegrated into a wide range of large or small ligaments, drops by the action of internal and external forces. The following investigation of this study focus on jet breaks up using an air-assist atomizer in cross flow conditions. In air-assist atomizers, by the exposure of a liquid jet into a high-velocity air-stream, the atomization is taken place because of the transported kinetic energy from gas to liquid flow, which generates strong shear forces in the ambient gas and provides the required energy to break the liquid into drops.

During the atomization process are distinguished two wider regions between liquid column and droplets, which form the spray. However, from a detailed analysis in atomization process has identified actually five breaks up regimes (Dumouchel, 2008), which we will discuss further below. In general, the spray production is constituted of three steps, the ejection of liquid flow, the part of a primary break-up and the part of a secondary break-up, as is illustrated in

Figure **1.1**. The first breakup region is called primary and takes place near the nozzle exit where the liquid drops are directly flowing out in the formation of a continuous liquid column, so

is developed the injected jet. It contributes to the initial conditions for the spread flow region. In this region, liquid jet is a function of the hole nozzle geometry, flow velocity, surface tension of liquid and physical properties of the two working fluids. The secondary breakup region, which is observed, is a further break-up of the liquid bulks and includes the droplets deformation. In this regime coexist the break-up of the liquid column, the drop collisions, and coalescence. Further disruption of some unstable large drops into smaller drops, which have been produced in an initial disintegration phase, this interruption is constituted the secondary atomization. Consequently, to the formation of secondary atomization region are contributed to the aerodynamic interaction and the shear forces from surrounding air. Aerodynamic forces act straight on the surface area of the liquid ligaments and drops, formed during primary atomization, to break them up further into smaller droplets (Hadjiyiannis, 2014)

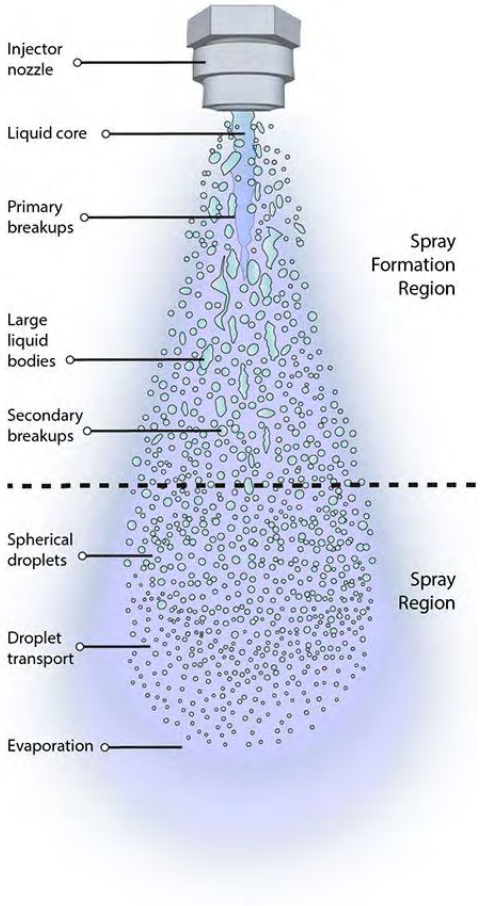

Figure 1.1: General scheme of spray formation (spray & imaging group, http://www.spray-imaging.com/spray-description.html

1.2 **Atomizers**

An atomizer is used to produce a spray or a gush of liquid and the atomization products are an effect of combination between flow conditions and geometry of atomizer. The operating principle is based on the interaction of high relative velocity between the liquid to be atomized and the surrounding air or gas. There is a range of different atomizers, each of them designed for a particular application, an appropriate range of flows or flow pattern, and to generate the desired droplet size and velocity distribution (N. Ashgriz, 2011), but the most common categories are pressure, rotary and twin-flow atomizers. Additionally, according to their geometry, atomizers are separated into types such as plain orifice pressure atomizers, dual orifice, simplex, duplex, square spray and other types **Σφάλμα! Το αρχείο προέλευσης της αναφοράς δεν βρέθηκε.**. In this project is used an air-assist atomizer which is fallen in the general category of twin-fluid atomizer and is ideal for representing the atomizing process of liquid fuels in continuous-flow combustion systems, such as turbine engines, where air velocities of this magnitude are usually readily available (Lefebvre & McDonell, 2017).

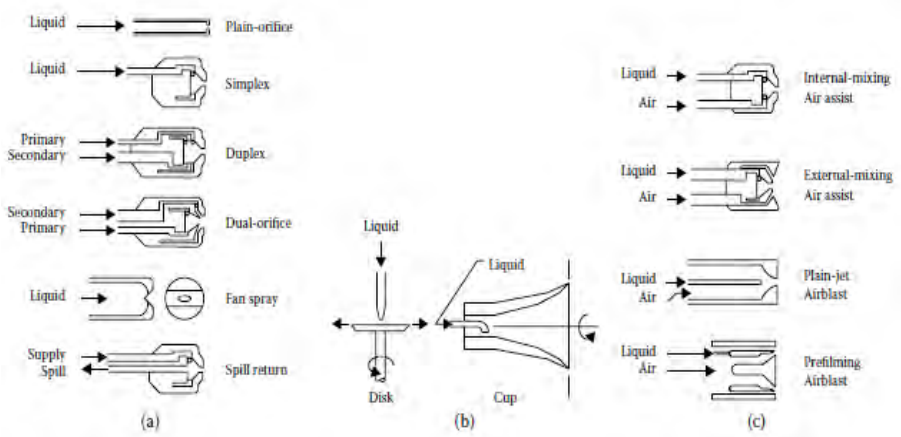

Figure 1.2: Different types of atomizers: (a) Pressure atomizers, (b) Rotary atomizers, (c) Twin-fluid atomizers (Lefebvre & McDonell, 2017)

Furthermore, nozzles can be divided into different categories according to their spray patterns which are generated from the nozzle. Three common spray shapes are the flat fan, full cone, and hollow cone spray. A typically spray angle is range from 20°to 120°degrees **Σφάλμα! Το αρχείο προέλευσης της αναφοράς δεν βρέθηκε.**. The characteristics of spray such as the impact area, flow rate and droplet size distribution differ from each nozzle.

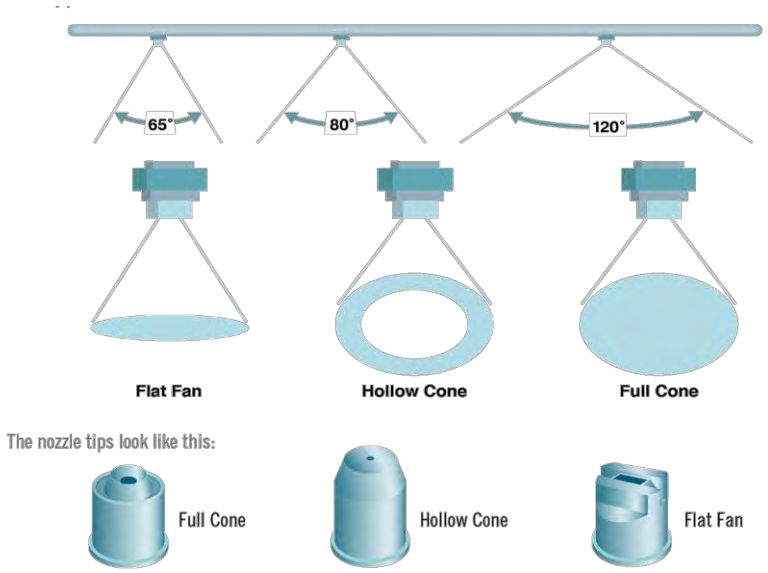

Figure 1.3 : Nozzle spray patterns and shapes (Hofman, V., & Solseng, E. (2004)

1.2.1 Air-Assist Atomizer

Air-Assist atomizer employs high- velocity air (>200 m/s) through the nozzle to achieve atomization. In general, air-assist nozzles require little mass air flow to operate, which make them suitable in atomizing systems that are required to operate with as little mass flow of air as possible. These types atomizers are ideally appropriate for atomizing liquid fuels in continuous air flow systems because they are suitable for the production of straight jets. The principal operating of the air-assist atomizer is based on the liquid discharge in an airstream flow of high velocity. They are categorized in internal-mixing and external-mixing types. Internal-mixing nozzles have the advantage of the wide flexibility and are particularly useful for atomizing highly viscous liquids. At the internal mix, gas and liquid are mixed within the nozzle before discharging through the outlet orifice **Σφάλμα! Το αρχείο προέλευσης της αναφοράς δεν βρέθηκε.**(a) (N. Ashgriz, 2011). External-mixing atomizers usually employ a high velocity stream of air or steam that flows from an annular nozzle and is arranged to impinge at some angle into a jet of liquid that is created at the center of the atomizer (Lefebvre & McDonell, 2017) **Σφάλμα! Το αρχείο προέλευσης της αναφοράς δεν βρέθηκε.**(b). The supply air is kept under pressure and must be fed when it is needed and not on an ongoing basis, this is the main difference from air-blast nozzles, where the air is supplied continuously. This class of atomizers gives the ability of using only supply liquid, hence a liquid spout is formed. The maximum spray angle in these atomizers is limited to about 60. This type of atomizer is recommended because of its advantage to avoid problems of back pressures through no internal communication between gas and liquid. It is important that this type

of nozzle can atomize high-viscosity liquids effectively. In this study is employed an external-mixing atomizer for the experiments in order to have only liquid flow.

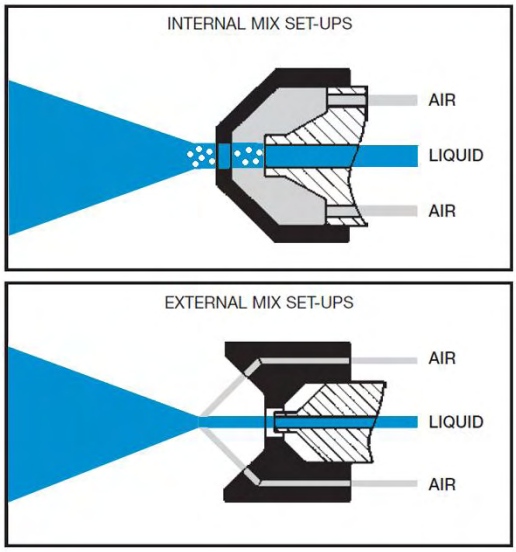

Figure 1.4: Air-Assist atomizer (a) internal mix atomizer, (b) external mix atomizer (PNR organization UK) http://www.pnr.co.uk/products/nozzles/spray-nozzles/atomiser-nozzles/classic-atomiser-nozzles/

1.3 Mechanism of Jet Development

1.3.1 Generally

It is primary importance to understand the mechanism of jet development and the growth of disturbances so that we can predict the liquid characteristics of the atomization products and the dynamic behavior of the liquid jet. In the progress of jet development downstream the exit of the nozzle, the disturbances on jet surface are increased continuously, which lead to disintegration into small and large composition of ligaments and drops. Both experimental and simulation investigations are driven by a desire to better understand the overall atomization process. Some knowledge of break-up regions and ligaments, drops size distribution is helpful to understand the jet development process. In an attempt to determine the type of atomization we should know both the break-up length and the uninterrupted liquid core of the jet length (Lefebvre & McDonell, 2017). Furthermore, the knowledge of drops velocities, ligaments break-up, size of drops and the volume flux distributions is required to characterize the structure of a fluid form. A typical spray formation includes a wide range of droplets sizes and ligaments which are randomly distributed in air volume flux. The challenge is to achieve specified characteristics in flow rate towards the development break up process. By saying specified characteristics we refer to liquid break up length which can be defined by the extension of the primary atomization region and includes the

mixture of sizes droplets, which are dispersed in downstream. It is important to predict some features of jets such as jet trajectories, penetration length, liquid jet length break up, drop sizes and their distributions in order to have the desired form of the jet for each of different operations. Consequently, in this way, we manage to accomplish the desired effects for each process such as in combustion engines. In this particular case, liquid jet injection and sprays are helpful to combustion process evolution, especially these days that a lot of attention is given in the reduction of combustion emissions and fuel consumption (Hadjiyiannis, 2014).

1.3.2 Non-Dimensional Numbers

In order to characterize the shape and penetration of the spray or a jet, we should determine drop velocities and size distributions. A wide range of parameters such as air pressure, flow out velocity, temperature and some others play an initial role in atomization process (N. Ashgriz, 2011). Therefore is needed to develop models that would describe the process. In an attempt to describe the correlation between the liquid flow and their properties in specific boundary conditions, has been generated the above nondimensional numbers, which are the Reynolds and Weber numbers related to the mass flow (N. Ashgriz, 2011). These numbers combine the aerodynamic forces which tend to deform the liquid interface and the surface tension forces which act to retain the initial shape, in order to characterize the flow. Depending on the mass phase, Reynolds and Weber numbers can be described for liquids and gases, using the equivalent liquid or gas properties and liquid or gas velocities (N. Ashgriz, 2011).

- The Reynolds number represents the ratio of inertial forces to viscous forces and is described from the equation (Reitz, 1987):

$$\text{Gas phase: } \mathrm{Re_g} = \frac{\rho_{g*} U_g *d}{\mu_g}$$

$$\text{Liquid phase: } \mathrm{Re_l} = \frac{\rho_l * U_l *d}{\mu_l}$$

- The Weber number represents the ratio of aerodynamic forces to the force of initial surface tension and can be described as (Reitz, 1987):

$$\text{Gas phase: } \mathrm{We_g} = \frac{\rho_g * U_g^2 *d}{\sigma}$$

$$\text{Liquid phase: } \mathrm{We_l} = \frac{\rho_l * U_l^2 *d}{\sigma}$$

The result of combination Weber and Reynolds number is to eliminate the velocity from equations and a new non-dimensional number becomes the Ohnesorge number.

- Ohnesorge number often known as viscosity number because relates the viscous forces to inertial and surface tension forces and is displayed in the above equation:

$$Oh = \frac{\sqrt{We}}{Re} = \frac{\mu}{\sqrt{\rho\sigma d}}$$

A large value of this number indicates a great influence of the viscosity and small values of Ohnesorge number means that the effect of viscosity is minimum. Although has to be made the assumption that the viscosity of ambient gas is small compared to that of the liquid. This number is often used to relate to free surface fluid dynamics such as dispersion of liquids in gases. Unfortunately, these dimensionless numbers are not adequate on their own to describe the atomization. In general, the discussion around the atomization process is based on the assumption of the high relative velocity between the liquids structures and the surrounding gas, but in situations with an extremely high relative velocity or a sudden change in velocity may be difficult to determine the process.

An important role in jets and sprays formation plays the ratio of mass flow across a unique area such as the nozzle exit surface. This ratio defines the mass flux.

$$\Phi = \frac{\dot{m}}{A}$$

An other parameter which related with an injection of a liquid jet into a crossflow stream is the liquid-to-air momentum flux ratio and is defined as the correlation between the mass flux Φ and velocity in gas and liquid:

$$q = \frac{\rho_l u_l^2}{\rho_g u_g^2}$$

The liquid to gas momentum ratio (MR) is defined as follows:

$$MR = \frac{\dot{m}_L}{\dot{m}_A} = \frac{\rho_L u_L^2 d^2}{\rho_A u_A^2 (d_G^2 - d^2)}$$

The numbers of (q) and (MR) signify the ratio of the liquid momentum ratio to the surrounding air momentum.

1.4 Factors Influencing Atomization

1.4.1 Nozzle Geometry

The size and frequency with which droplets and the round jet can be produced depending on the geometry of orifice and, more specific, on the pace of the liquid flow through the needle.

By saying, geometry of orifice we pertain to the needle diameter, the length of the injection orifice, the curvature of the orifice inlet, the angle which is formed in the exit of the nozzle and the shape that is shown how sharp or round is the edge (Arai, M., Shimizu, M. & Hiroyasu, 1991). Round edges orifices produces less turbulent liquid column, the jet disintegration is slower and produce higher spray penetration and better control to the process. All these parameters affect liquid penetration and break up, droplets size and the distribution of flux. The form of an internal flow and the final discharge orifice evidenced the importance of nozzle geometry on the atomization mechanism.

1.4.2 Liquid Properties

The liquid jet structure and the formed droplets are strongly influenced by the liquid properties, such as density, viscosity and surface tension and of course by the liquid and gas velocities. Some knowledge of working fluid properties is useful to choose carefully the appropriate fluid for the atomization process because of its viscosity determines the droplet size distribution. It is seldom possible to change the density without affecting some other liquid property. A use of a liquid with high viscosity decreases the Reynolds number and delays the development of any natural instability in the jet. It is desired the atomization process performed under normal and stable conditions because the viscosity of liquids changes at once with temperature, more specifically it decreases when the temperature of the liquid increases. Such information is essential in an experimental process. We should emphasize that low viscosity of water makes it good simulant for fuels, that's the reason why I used frequently in atomization. Pressure and temperature of ambient gas into which sprays are injected, affect the atomization too. An increase in the surrounding gas pressure will lead to production of large droplet sizes. Surface tension is another important parameter of liquid properties which plays an important role in atomization process because it represents the force that resists the development of the new surface area. To describe the correlation between the inertial force and the surface tension force is used the dimensionless Weber number. Commonly encountered surface tensions range from 0.073 kg/s^2 for water to 0.027 kg/s^2 for petroleum products. Accurate detection of pure liquids properties is shown that the surface tension decreases with the increase in temperature. This is illustrated in following Figure 1.5.

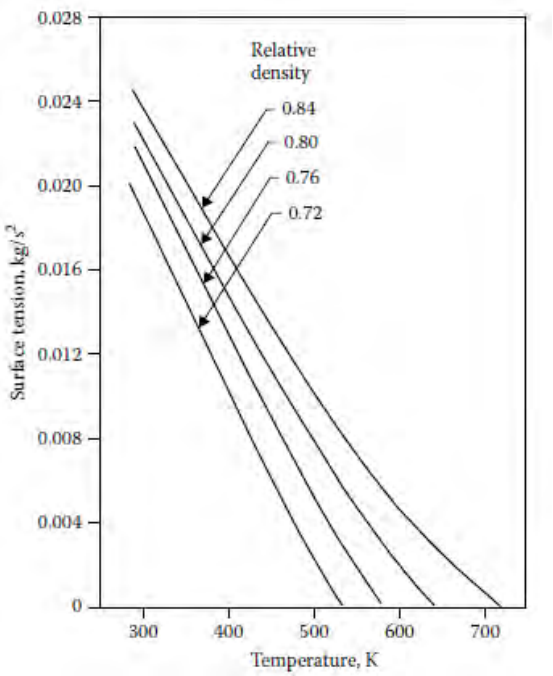

Figure 1.5: Relationship between surface tension and temperature for fuels of varying relative densities (Lefebvre & McDonell, 2017)

Moreover, an increase in fluid's viscosity lowers the Reynolds number and also decelerates the development of any instability in the jet. The apparent role of viscosity is to delay the break-up as it balances the force of inertia. The effect of viscosity on flow is varied from one type of atomizer to an other. Generally with an increase in temperature the viscosity of liquids decreases. Such information is essential in fuel oils processing where the heavier oils heat up when it is necessary to reduce pumping power and at the same time improve atomization. The successfully understanding of atomization behaviour is correlated with a well understanding of the physical properties of the used liquid.

1.4.3 Ambient Conditions

1. Pressure & Temperature

The ambient conditions are a major factor in the atomization process. By saying ambient condition included pressure and temperature of the ambient gas into which jets are injected. The ambient gas density is changed with temperature and pressure alternation. The mean drop size is strongly influenced by the ambient gas density. If the environmental pressure exceeds the normal atmospheric value, the mean drop size increases initially until a maximum value is reached and then slowly declines (Lefebvre & McDonell, 2017). The length of the intact surface decreases with increasing environmental pressure to a certain value. Furthermore, as the gas velocities relative to the droplet increase, the form of break-up changes. The different spray pattern which

generated by dissimilar atomizers affected uniquely by the ambient gas and generate different airflow patterns. External distorting forces which applying to a liquid jet are originated from aerodynamic forces which acting on the liquid surface. Faeth noted that for $\rho_L/\rho_G < 500$ the aerodynamic forces influence the atomization (Faeth, 1999) .In particular, the change in aerodynamic drag forces produced by a change in air density will affect the resulting spray pattern. In general, an increase in air density will cause the fluid jet pattern to adhere more closely to the streamlines of the atomizing air.

2. Effect Of Turbulence

Another factor of ambient conditions is the state of turbulence at injector outlet which interacts in atomization of the jet on a microscopic scale. The mixing rate and distribution of drops depend on turbulence. Thus the mixing rate is increased with the presence of turbulence. Usually, turbulent jets are atomized into smaller drops than in laminar jets.

3. Cavitation

Also, in nozzles of liquid atomizers is observed cavitations phenomena. Earlier investigations proved that the cavitations phenomena which exist inside the nozzle have an effect on the interface of the jet (Dumouchel, 2008). Cavitations phenomena which take place in a nozzle, should taking into account because contribute to the dissolution of the liquid jet. Actually, cavitation can be explicated as the process of forming a vapor-air pocket or bubbles as a consequence of lowering pressure into the needle of the nozzle(Sou, Hosokawa, & Tomiyama, 2007). It has been determined that strong turbulence in the nozzle hole, induced by cavitations phenomena, contributes enormously to the disintegration of the liquid jet. Observed four regimes at the cavitation process as illustrated in following Figure 1.6 for water and temperature condition T=292 K.

In an initial phase for $\sigma > 1.2$ and $Re<50000$ cavitation bubbles are not observed and in this phase the liquid has the form of "wavy jet". Increasing the Reynolds number up to $Re<64000$ and for $\sigma > 0.78$ cavitation bubbles regimes formatted in the upper of the needle of the nozzle. Next regime is called "super cavitation" and liquid jet atomization is intensified. Cavitation bubbles observed into nozzle and the exit of the nozzle is formed a spray with ligaments and droplets. Further increase of Reynolds and decrease of σ (surface tension) has as a result, the formation of "hydraulic flip" and "flipping jet" in which flow is separated at one inlet edge and not reattach to the side wall (Sou et al., 2007).

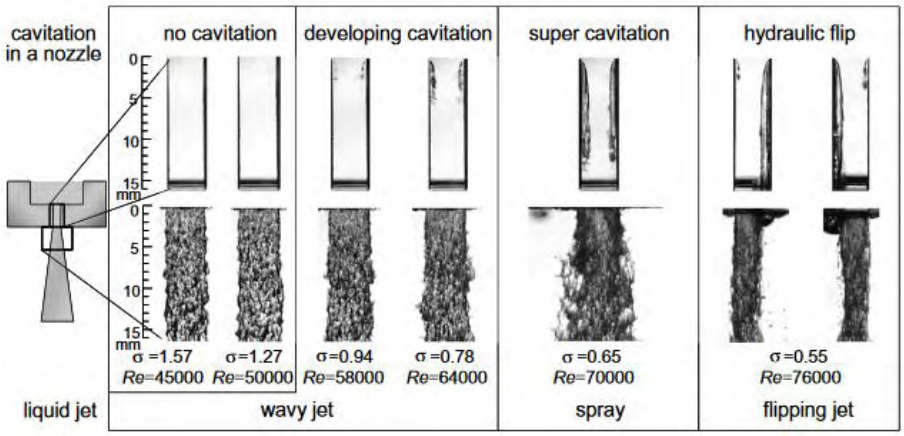

Figure 1.6: Cavitation in a 2D nozzle and liquid jet (Sou et al., 2007)

1.5 **Basic processes in atomization**

During the atomization a liquid bulk is converted into ligaments and small droplets. Before the last regime which is actually the atomization the liquid is disintegrated through different steps. In a foregoing discussion are investigated the factors which influence the atomization process, such the liquid viscosity, the velocity of the ambient gas, aerodynamic forces and surface tension. All these factors have direct relevance with the mechanism of liquid bulk disintegration. The variety of drop sizes produced in a spray depends on different types of formations and stages.

Assuming a liquid bulk is consist of continuous liquid droplets. An amount of larger droplets and ligaments which produced in the initial phases of the disintegration process are unstable and undergo in further splitting into smaller particles. In general, the atomization process is a result of interaction between a liquid and the surrounding air. This process involves many mechanisms, among which is the disruption of larger drops during the stages of atomization. In equilibrium conditions three pressures act on a liquid drop. In particular, the drop surface at any point stressed for internal pressure, p_I is just enough to balance the external aerodynamic pressure pA and the surface tension pressure pσ so that it is valid the equation (Lefebvre & McDonell, 2017) :

$$p_I = p_A + p_\sigma = \text{constant}$$

If aerodynamic pressure changes at any point on the surface of the liquid, this change is corresponding to other change of pressures so that the internal pressure remains constant. If the aerodynamic forces on drop are so strong, then a break on the surface makes an appearance.

1.5.1 Static Drop Formation

The most simple and elementary drop formation is the quasi-static case of the hanging drop. This is the instance of the slow discharge of a liquid bulk into drop when only the gravity force on the liquid. In this case of drop formation the liquid is pulled away from its initial connection and the droplets are formed when the gravity force exceeds the essential surface tension force. This type of drop formation entails large drops and low flow rates Figure 1.7

Figure 1.7: Static drop formation and dripping regime (Ain, 2012)

1.5.2 Drop Breakup In Flowing Air

In a liquid breakup in a flowing stream, the atomization process depends on aerodynamic pressures, viscous stresses and surface tension. In air stream regimes, for any given liquid, the initial breakup condition is succeeded when the aerodynamic drag force becomes equal to the surface tension force. That given by the following form:

$$C_D \frac{\pi D^2}{4} 0.5 \rho_A U_R^2 = \pi D \sigma$$

The maximum stable drop size for a relative velocity is given by:

$$D_{max} = \frac{8\sigma}{C_D \rho_A U_R^2}$$

When a drop is abruptly exposed to a high-velocity relative gas stream, then is disintegrated in an array of multi-step up to final breakup into a drop of various sizes. As is illustrated the initial drops are blown out into a thin hollow bag holded in place to a rim and into variety of drops sizes Figure 1.8.

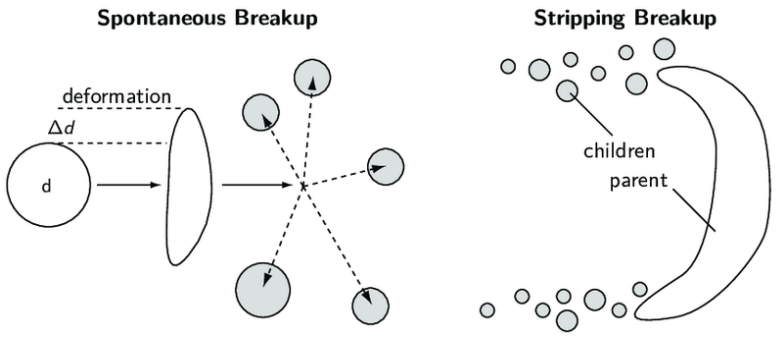

Figure 1.8: Drop breakup process in flowing Air, https://www.researchgate.net/figure/Breakup-Modes-Spontaneous-breakup-leads-to-immediate-disintegration-of-the-parent-drop_fig4_272063743

1.5.3 Disintegration of Liquid Jets

Prime importance is the way in which the jet is interrupted and the development process. Disintegration of a liquid bulk has been in the centre of attention for many investigators such Savart who showed that if the jet diameter is kept constant, the length of the continuous part of the jet is directly proportional to jet velocity. He also observed that, for constant jet velocity, the length of a jet is directly proportional to its diameter (Savart, 1833). Meanwhile, Rayleigh employed the method of small disturbances to predict the conditions necessary to cause the collapse of a liquid jet issuing at low velocity (Rayleigh, 1878a). He calculated the potential surface energy on the disturbed column. As a result, surface tension forces have an effect on a liquid jet and tend to make it unstable to any axisymmetrical disturbance whose wavelength satisfies the inequality.

$$\lambda > \pi d$$

Consequently, if a disturbance occurs on a laminar jet with a wavelength greater than its circumference, will grow and a single drop will be produced per wavelength. Rayleigh mathematical treatment of the breakup of jet presented that the average drop size is near twice the diameter of the undisturbed jet and actually is

$$D = 1.89d$$

Rayleigh theory is generally accepted in the later investigation and the initial regimes in atomization process are approximated the Rayleigh state. The following picture Figure 1.9 (a) is observed the appearance of the jet in this region. During the axisymmetric drop formation usually,

are formed small single drops between the large drops which call satellite and fretted among the flow Figure 1.9 (b).

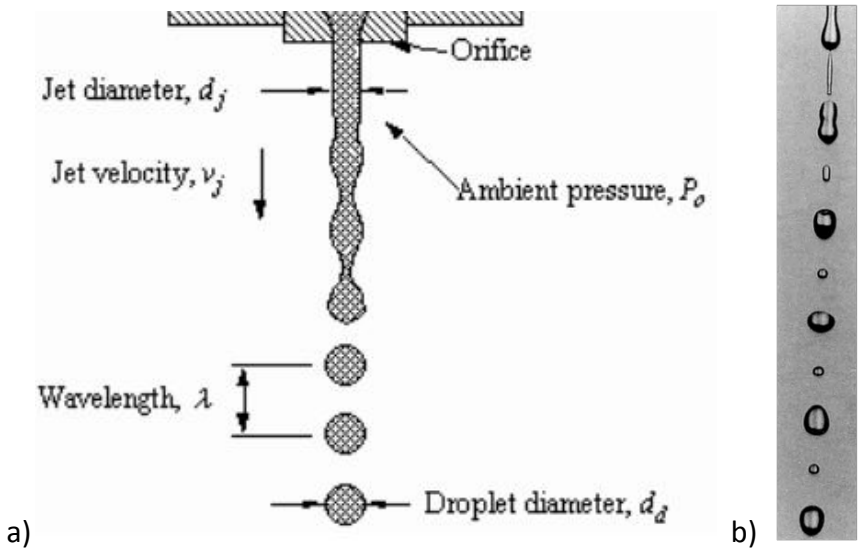

Figure 1.9: a) Disintegration of a liquid jet , b) Axisymmetric drop formation and satellite formation (Courtesy of the Royal Society handbook)

Weber extended Rayleigh's analysis including viscous liquids and low jet velocities. The outcome of this investigation reveal that the minimum wavelength, which is a result of disturbance, is the same for both viscous and non-viscous liquids, but the optimum wavelength is greater for viscous liquids. Furthermore, he found that ambient air friction decreases both the minimum wavelength and the optimum wavelength for drop formation. Therefore, the relative air velocity reduces the optimum wavelength for the jet breakup. Haenlein investigates the disintegration of liquid bulk and define four distinct regimes. (Haenlein, 1932a). First was the drop formation without the influence of air, second the drop formation with air influence, third drop formation due to waviness of the jet, fourth the complete disintegration of the jet, final atomization Figure 1.10.

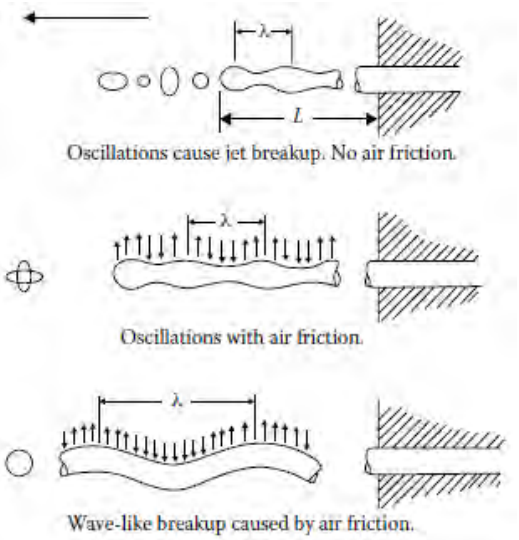

Figure 1.10 : Mechanisms of drop formation. (From Haenlein, A., Disintegration of a liquid jet, NACA Report TN 659, 1932.)

The non-dimensional numbers usually use to describe the categorization of the anticipated phases of primary breakup and based on these numbers is divided into different types of break up (Ohnesorge, 1936). The previous theory from Ohnesorege was enhanced by Reitz with the introduction of a differentiation between first and second wind induced breakup (Reitz, 1987). At first, Ohnesorge relates the interaction between Reynolds and Ohnesorge number and establish that the mechanisms of the jet breakup could be organized into three regions depending on Reynolds number and on the rapidity of drop formation. Low Re region, intermediate Re and high Re region are illustrated in the following Figure 1.11.

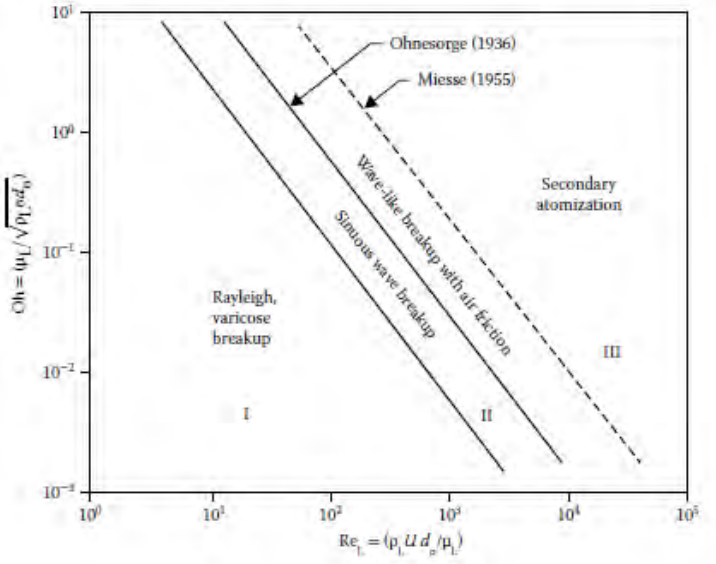

Figure 1.11: Classification of modes of disintegration. (From Ohnesorge, W., Z. Angew. Math. Mech., 16, 355–358, 1936.)

1.6 Breakup Regions

1.6.1 Primary Breakup

Primary breakup is the centre of interest for many studies by numerous authors. Four distinguished modes of the primary breakup were observed in mechanisms of liquid jet break up. (Reitz, 1987) improved (Ohnesorge, 1936) investigation and he showed that, as the liquid injection velocity is progressively increased then are distinguished four regimes of a breakup. Generally, the identified regimes are based on a combination of inertia of liquid, surface tension and forces of aerodynamic acting on the jet.

1. Rayleigh Breakup

Rayleigh breakup regime is observed at low jet velocity and liquid bulk is disturbed by a small axisymmetric perturbation, which promotes an axial-symmetric oscillation at the surface. The perturbation produces wavelengths which when becoming equal to the jet diameter the liquid column leads in breakup and drops are detached from the jet. At this stage of primary breakup only the surface tension plays an important role in the breakup characteristics. The obtained droplets are equal size or even larger than the diameter of the primary jet (Kadocsa, 2007).

2. First Wind-Induced Breakup

As the Weber number progressively is increased, but at the same time all the boundary conditions remain constant, the aerodynamic forces which acting on the surface of the liquid column become more powerful. The pressure distribution resulted from the flow around the surface perturbations contribute to the breakup process. The produced drops are close to a similar radius as the jet radius or a little smaller.

3. Second Wind-Induced Breakup

The second wind-induced regime takes place near the exit of nozzle and is characterized by a chaotic distribution. A further increase of Weber number means that the turbulence effects and the aerodynamic forces contribute to the breakup. the processes of the first wind-induced breakup still occur, but in a larger extent, and more rapidly, providing droplets (Kadocsa, 2007). At this regime, small droplets are produced and the remaining large fragments disintegrated further to droplets from the jet surface.

4. Atomization

The liquid jet abruptly right starts to get distracted along the entire jet cross section at the exit of the nozzle hole. It means that the unbroken liquid jet section, the symmetric, undisturbed liquid column characteristic to the former three breakup regimes in a decreasing extent with an increase

of Weber number, is either absent in this case or under circumstances exists in a very short length. In this case, the resulting drops have diameters much smaller than the jet diameter.

Below is illustrated the corresponding of four regimes of a liquid bulk breakup, which describes the length of the unbroken jet as a function of jet velocity and at the same time shows the respective Weber number of each regime Figure 1.12.

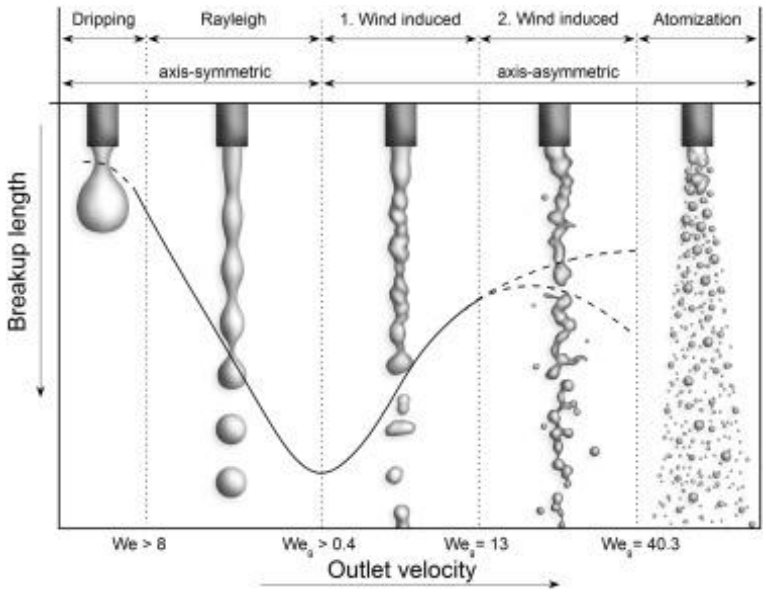

Figure 1.12 : Breakup length as a function of outlet jet velocity (Journal of Pharmaceutical Sciences, https://www.sciencedirect.com/science/article/pii/S0022354916419453

The initial phase is the dripping flow which is observed in very low velocities and no jet is formed. A gradual escalation of jet velocity militates growing axis-symmetrical oscillations on the surface of liquid jet. The unbroken length continuously increases until the drop formation, which has diameter larger than the orifice hole diameter. The breakup regime of flow that has already referred calls Rayleigh regime.

When the jet velocity increases then at the same time the breakup length increases linearly up to a maximum limit. During the first wind-induced regime, the pre-existing forces of the previous Rayleigh regime are augmented by the presence of aerodynamic forces and are formed droplets size in the range of the nozzle. The relevant parameter is the gas phase Weber number We_g, which describes the influence of the surrounding gas phase.

In the second wind-induced break-up regime, the flow inside the nozzle becomes turbulent. Jet break-up now occurs due to the unstable growth of short wavelength surface waves that are initiated by jet turbulence and amplified by aerodynamic forces due to the relative velocity between gas and jet. The diameter of the resulting droplets is smaller than the nozzle diameter, and the break-up length decreases with an increasing Reynolds number (Sutradhar, 2012).

The final regime is the atomization, where spray forms immediately after the jet leaves the nozzle. The resulting droplets are much smaller than the nozzle diameter and the disintegration process depends on the flow conditions inside the nozzle. The above results of breakup regimes are summarized on Table 1.

Table 1: Jet breakup regimes (Lin and Reitz,1998 and Atay I., Gordon, L., and Richard, 1987)

Type of Regime	**Jet velocity U_0 m/s**	**Break up length L in terms of L/d**	**Diameter of drop, D**	**Weber number**
Rayleigh jet Break up Regime	0 - 5	10 – 110	D > d	$We_L > 8$ $We_g < 0.4$
First Wind Induced Breakup Regime	5 - 10	110 – 60	D = d	$0.4 < We_g < 13$
Second Wind Induced Breakup Regime	10 - 18	60 – 100	D < d	$13 < We_g < 40.3$
Atomization Regime	>18	0	D << d	$40.3 < We_g$

1.6.2 Secondary Breakup

The secondary atomization begins when the initial liquid formation and structures are turned into a liquid stream and become unstable. After the primary breakup follows the secondary breakup atomization, as it is used to referred, where the initial structures from the primary atomization are disintegrated further to multiple droplets, as a result of the interaction with the surrounding flow. These fluids parts from the primary breakup regime are usually not stable and hence are leaded to further stage of breakup until are formed the final drops. The main cause of secondary breakup phenomena is mainly through the aerodynamic forces which acting on surface of fluid. Therefore, the relative velocity of the droplet and the surrounding ambient gas stream are the most important factor in the breakup mechanism. Weber number is used to determine the different phases of secondary atomization Figure 1.13.

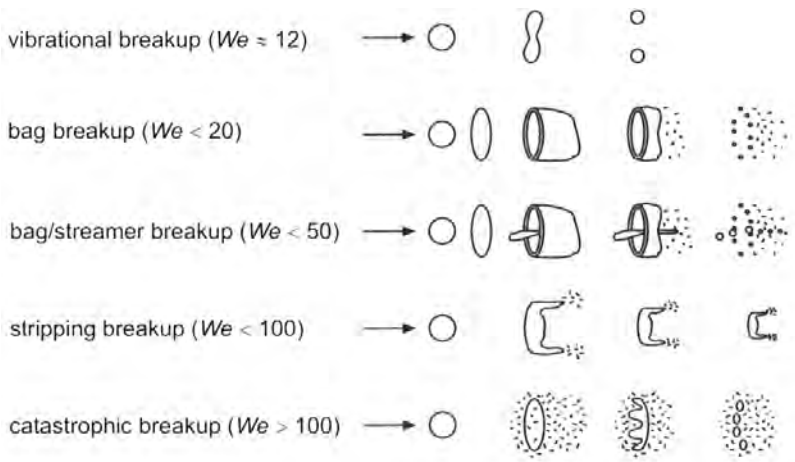

Figure 1.13: Drop breakup regimes according to Wierzba (Wierzba, 1993)

Above are illustrated the most common breakup modes in secondary atomization. The first state is the vibration breakup where initial drops disintegrated into a few relatively large drops through the oscillation in the surface. That happens for Weber number below the critical (We ≈12). Increasing the Weber number up to We<20 then the drops deform to a flat disk shape and the disk becomes thinner in the radial direction. Due to pressure forces is formed a hole on the surface of the thin disk and afterward break up into many small drops. This process is called bag breakup. For even higher Weber number up to We<50 the process of drop formation is similar with the bag breakup. When Weber number become We<100 then stripping breakup is observed, where drops in this case deform to an oblate spheroid. Then with the effect of viscous forces from the ambient gas sweep the rim of the drop downstream and break off small droplets from the stretched rim later on (Kekesi, 2017). In flows with very high Weber numbers We>100, the drop suddenly breaks up to a large number of small drops. This phenomenon is referred to as catastrophic breakup (Kekesi, 2017). During sprays atomization, all these breakup mechanisms exist, however the majority of the disintegration processes usually take place near the nozzle at high Weber numbers.

1.7 **Cross flow**

Jet in cross flow has been the subject of various investigations, both experimental and computational. One case of practical importance is fluid injection into a cross flow stream either into a co flowing or contra-flowing stream air. Into a uniform gaseous cross flow a round liquid jet is allowed aerodynamic forces and pressures on surface, hence tend to be distinguished in smaller particles. A typical round non-turbulent liquid jet into a cross flow air and its structures is shown in Figure 1.14.

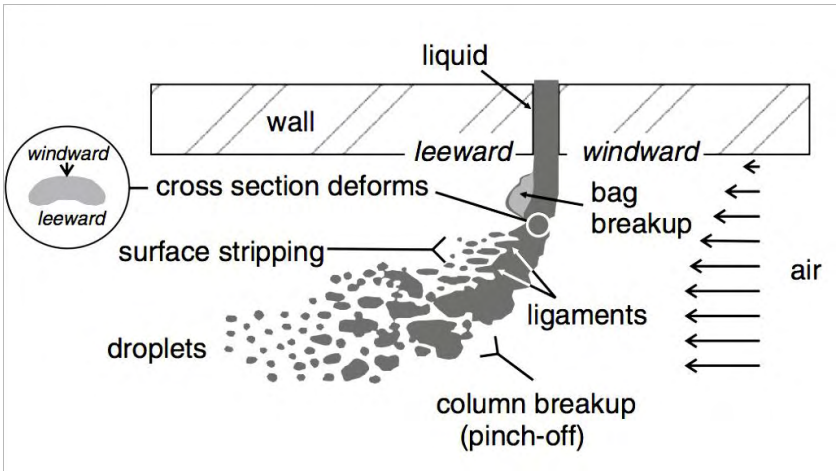

Figure 1.14 : Round liquid jet development into a gaseous cross-flow (Sina Ghods, 2013)

The injected jet tends to follow a parabolic trajectory under the affect of gaseous cross-flow. This formation is caused by reduced pressure along the sides of the jet , after the exit of nozzle, and due to acceleration of the gas across the liquid column at the same time (Sina Ghods, 2013). It is important to mention that the exposed side of liquid column, which is windward to the air stream is allowed strong forces and higher pressure than the leeward side, where establishes lower pressure wakes. Increased forces cause for a breakup on the liquid bulk surface and then the initial liquid column disintegrate into small and large ligaments. Further down the column is breaking up totally and the ligaments are distinguished into various sizes of droplets.

When a spray injection is oriented to the airflow, the larger drops penetrate farther into the airstream and the spectrum of drop sizes which is produced in the flowing airstream is skewed radically Figure 1.15 (Lefebvre & McDonell, 2017).

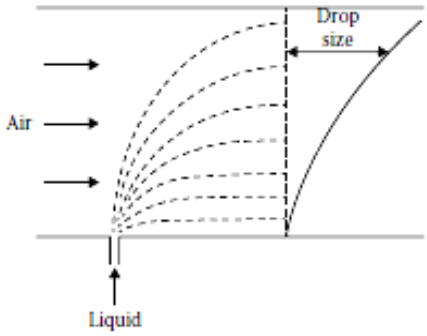

Figure 1.15: Influence of cross-stream airflow on drop size distribution (Lefebvre & McDonell, 2017)

In particular, the cross-flow atomizers produce a spray from the interaction of the vertically liquid jet with the cross-flow steam. The impact of the cross-flow normal to the jet trajectory causes instabilities on the surface that become inherently three dimensional as they move tangentially

around the jet centreline as well as in the direction of the cross-flow. The gaseous flow break the liquid entirely into fines drops and some large structures such big droplets and ligaments are shaped along of smaller droplets. A droplet has the tendency to follow the direction of crossflow air and this drifting characteristic increases with decrease in its size. Hence the larger droplets tends to follow their initial trajectories into crossflow air stream whereas the smaller drops lose gradually their initial direction and entrain to the crossflow air trajectories (Sallam, Aalburg, & Faeth, 2004).Is observed two separate flows of drops which follow different trajectory and consist of larger drops the first and of smaller drops the second that happens for low momentum ratio cases Figure 1.16. Overall, the spatial bifurcation is attributed to a combination of factors such the presence of large ligaments and droplets near the exit of nozzle, the secondary breakup formation and the differential dispersion in small and large drops. The smaller droplets float away into the crossflow stream at much lower elevations, while the larger droplets follow the initial trajectories and tend to penetrate farther into the crossflow. A typically spray trajectory in cross flow is characterised from an initial non-linear part which after a specific distance downstream tends to become linear. Due to the initial momentum the droplets surge vertical to flow and then entrained from stream flow, hence the curve path is non-linear. A progressive loss of vertical momentum of the droplets has as a result curve path to tend to become linear and this change is very gradual. Two factors are most important and affect the trajectory of droplets which injected vertically into a crossflow. The first is the initial momentum and the second is the effectiveness of the drag forces induced by the air stream. Drag depends on projected surface of the drop in stream flow and the momentum depends on mass of drop. Both of these factors depends on diameter of droplet and hence the larger droplets get least affected by air flow and penetrate furthest into the air stream. Whereas the smaller drops are drifted easier along the crossflow and their path direction is at much lower elevations. In attempt to describe better the trajectories of droplets has been employed an empirical correlation dependence on momentum flux ratio (q). Such a multi-variable regression algorithm was proposed by (Chen, T.H., Smith, C.R., Schommer, D.G., and Nejad, 1993),(Becker, J. and Hassa, 1999), (Ross, 2009) and many other researchers, who tried to correlate the dependence of the jet penetration and the momentum ratio (q) with the liquid jet path. Nevertheless, most recent investigators propose a logarithmic or a polynomial functionality to fit the trajectory path that a jet tends to follow. Therefore, some of the most common used functions to describe jet trajectories are:

1. $y = ax^2 + bx + c$ (2nd degree polynomial)
2. $y = bx^m$ (power law function)

The results of the experimental data is related with the numerical outcomes of the derives equation and they seem to be in good agreement with real trajectories (Sallam et al., 2004).

Figure 1.16: Phenomenon of spatial bifurcation of the spray in cross flow (for low GLR)(Sinha, Surya Prakash, Madan Mohan, & Ravikrishna, 2015)

The present study focuses on cross-flow investigations because of their wide range of application in the engineering field and aims at developing a cross flow atomizer. Because of the complex of cross-flow atomization, many researchers have been carried out for better understanding of spray structure. Some information on the expected spray structure is useful to understand better the mechanism that disintegrates the discharged liquid jet in a vertically cross-flow steam. An example is the diameter of the liquid jet exit can determine the turbulence of liquid jet and therefore the downstream products of atomization process. It is important to assess the different parameters affecting the trajectory for a wide range of liquid and cross-flows. In general, were identified three different mechanisms of atomization in cross-flow droplet formed, film surface atomization because of aerodynamic instability and film break-up at channel exit

1.8 **Similar investigations**

A short summary of the investigations and authors contributions is provided in the present section. From the nineteenth century significant research has been performed in spray atomization process and many investigations have been focused on identification of the mechanism and characteristics of the liquid jet breakup. Some of the most important studies on liquid atomization are carried out from (Faeth, 1999) who emphasized on understanding of primary and secondary breakup, on breakup outcomes as well focused on breakup due to shock wave disturbance. Moreover Faeth, 1995 found out that spray properties including criteria for the onset of breakup are strongly influenced by the degree of flow development and the presence of turbulence at the exit. Similar investigations were conducted from (Lefebvre, 1989) who defined the atomization regimes and associated each atomization regime to a typical flow structure, (Reitz, 1987) investigation shows an explicitly relation between liquid injection velocity and breakup regimes

and (Weber, 1931) extend the Rayleigh theory by taking into account the liquid viscosity, the jet velocity and the surrounding gas that introduces aerodynamic forces. Special attention is given from (Sallam et al., 2004) in breakup liquid jets in gaseous crossflow who extend the studies of (Mazallon and Wu), determined breakup properties and indicated that there are useful general analogy between the primary breakup and the secondary breakup of drops subjected to shock wave disturbances. Parallel to foregoing investigations there are significant researches which were useful to better understanding of atomization process. Such investigations were carried out from (Sou et al., 2007) who attended to effects of cavitations in a nozzle, classified the cavitations into regimes and shows the factors which are strongly affected to cavitations and liquid jet. In the recent past the primary break up process was investigated by (Wu, 1997) who classified the breakup regimes of a liquid jet in cross-flow using the Weber number (We) and the momentum flux ratio (q) and (Mazallon, 1999) who indentified the breakup regimes with Weber and Ohnesorge numbers. Furthermore the shadowgraphy method that based on image collection with high-speed cameras was employed from (Becker, J. and Hassa, 1999),(Wu & P.-K., Kirkendall, K.A., Fuller, R.F., Nejad, 1997) and many others recent researchers. Several authors suggested procedures to predict the trajectories of liquid jet in cross flow conditions. For this purpose have been built empirical and functional models of jet trajectories based on experimental data by investigators such (Chen, T.H., Smith, C.R., Schommer, D.G., and Nejad, 1993),(Wu & P.-K., Kirkendall, K.A., Fuller, R.F., Nejad, 1997),(Hadjiyiannis, 2014),(Sinha et al., 2015).

1.9 **Aim of the Thesis**

The instability and the breakup of a liquid jet are of primary importance especially in aviation applications(Lefebvre, 1989). Therefore, there is a need to study in detail the formation and behaviour of a liquid jet in gaseous cross flows, such as found in aviation engines. The scope of the current study is to investigate a liquid jet in a cross-flow gas stream and to identify the characteristics of the deflected jet for a range of liquid and air flow-rates. The present research focuses on a range of values of liquid flow rates and cross-flow conditions, which differ from the already existing investigation conditions that previous researches has employed. Water, which was employed for the experiments, has similar density and viscosity with light fuels such as kerosene and we can assume that the experimental process is a reasonable simulation of the way a liquid jet injected in a gas turbine engine behaves. Special attention is given on the liquid jet characteristics as it penetrates into the gas cross flow. The main focus is on the representation of the recorded trajectories. Also, effort was made to identify the penetration length, the penetration along the gas axis and the total length of jet until the first break up that is referred as primary breakup. The accuracy of the results was quantified using statistical methods. Additionally, the

present study focuses on image processing of the experimental measurements and for this reason a lot of work on shadowgraphy method and image processing is presented in the following chapters. Finally, special attention is given in understanding, how the different conditions influence the liquid jet characteristics and identify the dominant parameters.

2. Experimental Arrangement

2.1 Introduction

The experimental investigation was carried out in a test facility where a liquid jet from an air-assist atomizer was injected into a gaseous cross flow. In the following chapters the experimental arrangement employed in this investigation is presented in detail. The components that are required to setup the experimental facility and their characteristics are described below. The detection techniques, analysis and test conditions of atomization process are expatiated in chapter 3. This study employed the continuous shadowgraphy imaging technique where many instantaneous images are captured in order to observe the atomization process and breakup mechanisms. This method was used by many researchers such (Wu & P.-K., Kirkendall, K.A., Fuller, R.F., Nejad, 1997), (Sallam et al., 2004) and (Mazallon, J., Dai, Z., Faeth, 1999) in order to investigate the breakup of the liquid jet into a subsonic wind tunnel for different conditions. This optical technique is used in order to measure the instantaneous liquid jet characteristics.

2.2 Description of Experimental Arrangement

The experimental setup consists of a number of components connected in series Figure 2.1. A centrifugal fan is used to generate the gaseous cross flow. The purpose of the blower is to increase the air velocity into a section of cylindrical plastic tube ⌀12. The atomizer is located 5cm downstream of the exit of the cylindrical tube section and is mounted on a custom support made by a 3D printer. The atomiser injected the liquid jet into the subsonic cross flow. The atomizer is of the external mixing type. Straight flow is desired for the experiment, hence a honeycomb is used at the inlet of the tube section to straighten the gaseous flow. The air velocity is measured by a TSI anemometer. The anemometer sensor is supported on a metal base, and the sensor placed in front of tube exit normal to air flow to measure the velocity profile. During the tests the velocity across the main diameter of the tube exit was recorded. The liquid was placed in a pressure tank the pressure inside the tank was controlled by a high mass flow pressure regulator from which it was fed to the atomizer to produce the liquid jet. The test section and the spray position were designed to provide an unobstructed view of the liquid jet to be captured by the camera. A camera and a LED lamp which was the continuous light source behind the spray is used for the shadowgraphy imaging method to observe the liquid jet trajectory. The instantaneous images were recorded by a monochrome camera. The camera model is Allied Vision MAKO U-503 with 2592 × 1944 resolution. A detailed description for each of the experimental arrangements is given below

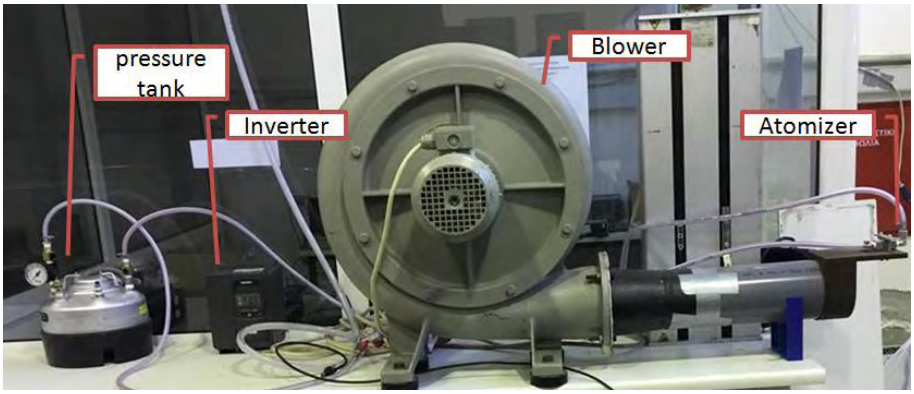

Figure 2.1: Experimental arrangements

.

Atomizer

The atomizer is placed at the edge of the exit of the cylindrical tube, secured on a custom base built by a 3D printer which is tightly fitted at the exit of the tube, and immersed in the cross flow stream which entrains the liquid jet. The atomizer is of the external-mixing air-assist type, model Spraying Systems 1/8J and 1/4J Series, SUE15B. In the external-mixing type atomiser the liquid and air streams are mixed outside of the nozzle, Figure **2.2**a,b, in contrast to the internal mixing type where the gas and liquid are mixed inside the nozzle. The advantage is that the air and liquid flow rates can be controlled independently. This type of atomizer offers the ability to conduct an initial experiment without the presence of supply air and to produce only a round liquid jet from the nozzle. The liquid and compressed gas are mixed externally to produce a completely atomized spray. Furthermore, the external mix atomizer cap Figure 2.2(c) is designed to produce a flat spray pattern Figure 2.3.

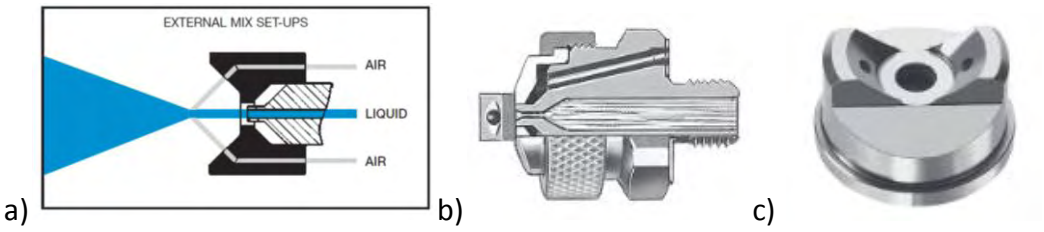

Figure 2.2: (a) Air and liquid external mix atomizer (PNR organization UK) ,(b) External mix with pressure set-ups, c) External mix air caps (Section F – Air Atomizing Spray Nozzles), https://www.spray.com/v1/cat70/cat70pdf/ssco_cat70_f.pdf

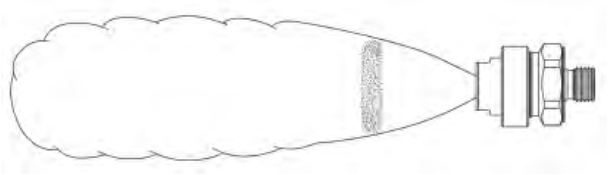

Figure 2.3: External mix atomizer with flat spray pattern (Section F – Air Atomizing Spray Nozzles) https://www.spray.com/v1/cat70/cat70pdf/ssco_cat70_f.pdf

Liquid supply system

In this study, a pressure tank is used for controlling liquid mass flow rate. The pressure tank, Spraying Systems 22140, is constructed from stainless steel and the pressure inside the tank can be regulated be a pressure regulator from 0.3 to 8.5 bar. Operating temperature range is 2°C to 93°C. The role of pressure tank is to supply of liquid to the atomizer. The pressure tank is shown in Figure 2.4.

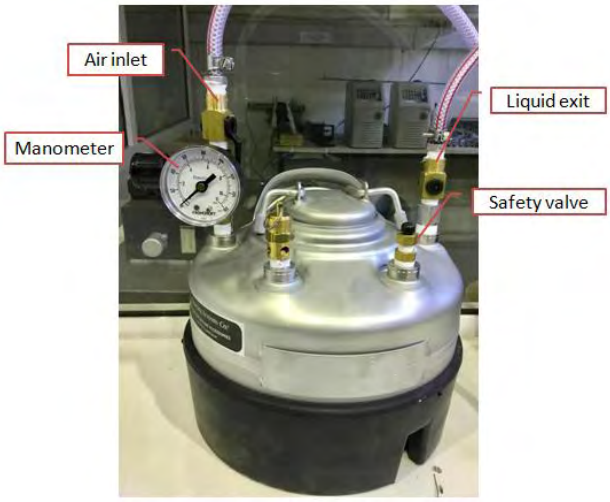

Figure 2.4: Liquid pressure tank (Section F – Air Atomizing Spray Nozzles)

Camera

A digital camera, allied vision model mako U-503 Figure 2.5 is employed for the liquid jet imaging. Mako U-503B is a monochrome USB3 Vision camera with the ON Semiconductor (Aptina) MT9P031 CMOS sensor and sensor size 1/2.5 with rolling shutter. The resolution is 2592 × 1944 pixels, the maximum frame rate at full resolution is 14 fps .

Figure 2.5: Allied Vision Mako U-503 camera

Blower

A centrifugal blower is used in this experiment to generate the gas crossflow. This device is powered by an inverter which controls the blower motor speed. The type of blower is Siemens D-97615 (Figure 2.6).

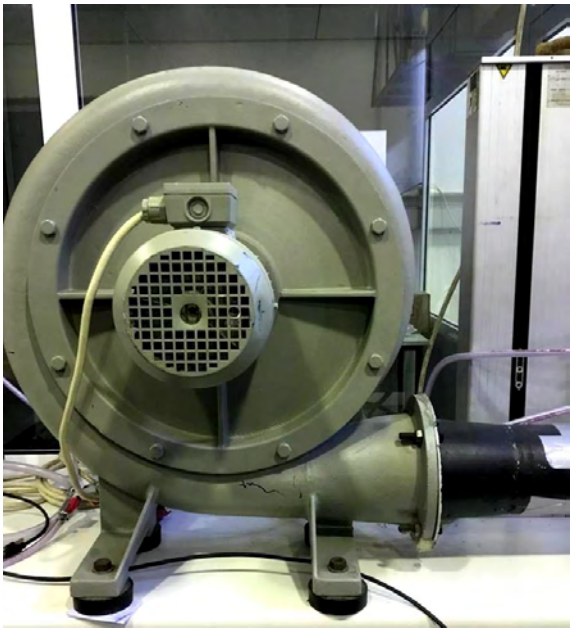

Figure 2.6: Centrifugal fan (Blower)

Honeycomb

A flow straightener, sometimes called a honeycomb, is used to straighten the air in the tube which is used in the experimental arrangement. The purpose of the honeycomb is to reduce the lateral velocity components caused by swirling motion in the air flow during entry into the tube. This configuration ensures that the gas exits the tube with laminar plug flow. The cross-section shape of the honeycomb cells is cylindrical.

Figure 2.7: Flow straightener (Honeycomb)

ABS Plastic Base

For the placement of the atomizer, a custom base was designed in Solid Edge (Figure 2.8.) software and was manufactured by 3D printing. The atomizer was secured on the plastic base so it remained stable during experiments.

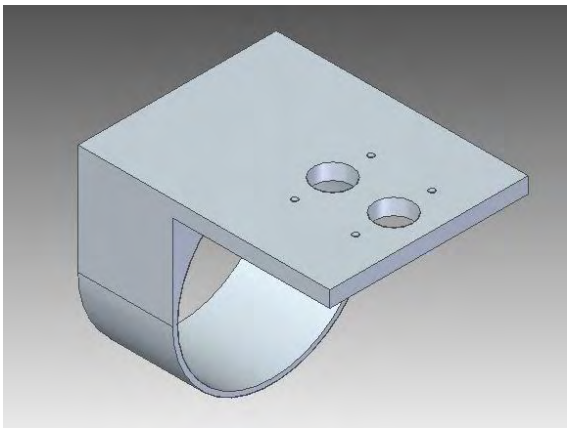

Figure 2.8: Plastic base designed in CAD software and printed in 3D printer

3. Experimental Methods

3.1 Introduction

Shadowgraphy is a widely used and reliable method to observe the spray atomization process and is especially suitable for visualizing droplets, moving particles and other liquid structures. This method is appropriate to observe the jet growth and its structures, especially the liquid length breakup, the wavelengths of column, the trajectories of the droplets, the size of the droplets and others characteristics of the atomization process. Several previous researchers such (Becker, J. and Hassa, 1999(Wu & P.-K., Kirkendall, K.A., Fuller, R.F., Nejad, 1997) adopted the shadowgraphy method in order to observe liquid jets or sprays. The present investigation is based on this technique which was employed to measure the liquid jet length in primary breakup, to calculate the trajectories, to measure the penetration length of jets and several other characteristics of jet breakup. A large number of instantaneous images are recorded in order to define the jet structures. The processing of a large number of instantaneous images results to reliable average values of the characteristics of the liquid jet under each specific test condition. This method is based on high resolution imaging with light illumination and is independent of the shape and material of the particles. A monochrome camera records the instantaneous images, hence structure of spray and droplets size can be observed. An LED lamp is the light source and provides continuous background illumination which scatters and refracts on the water liquid structures continuously. Initially, the LED lamp was placed directly opposite to the camera and the camera. This approach failed because it did not provide uniform background illumination across all of the imaged area. Hence, a white panel was employed as background on which the light from LED lamp was direct on and a uniform background illumination appropriate for the experiment was produced. An advantage of continuous illumination is that the liquid jet images can be captured at any frequency that the camera can operate at while if pulsed laser shadowgraphy illumination was used the camera would have to be synchronised to the laser pulse frequency.

The experiments, focus on the primary breakup process. The main interest of this study is the investigation of the primary breakup characteristics and trajectory of a round liquid jet into a gaseous crossflow.

3.2 Experimental Test Conditions

The present study was carried out under various flow conditions in order to observe, the behaviour of jet under different flow condition and identify how the breakup of the liquid jet was affected. The employed liquid for the experiments is purified water which is a low viscosity liquid

and has almost similar viscosity with kerosene (0.00164 Pa*s), therefore the results for the high velocity crossflow are appropriate for gas turbine engines. The test liquid properties are summarized in **Σφάλμα! Το αρχείο προέλευσης της αναφοράς δεν βρέθηκε.**.

Table 2: Test liquid properties

Liquid	Density [Kg/m^3]	Viscosity [Pa*s]	Surface tension [N/m]
Purified Water	999.70	0.001306	0,0742

The nozzle diameter is 0.5 mm. The tube diameter which supplies the gas cross flow is 120mm. The experimental flow conditions are summarised in Table 1Table 3. The air pressure in the pressure tank is measured by a manometer. For all cases the nozzle diameter and tube diameter remain constant while the crossflow air and liquid jet velocity vary. The crossflow velocities were measured by an anemometer and presented later. The combination of 4 pressures in the feed water (0.25, 0.5, 0.75, 1.0 bar) and 5 blower operation frequencies (10, 20, 30, 40, 50 Hz), resulted in 20 different experimental conditions.

Table 3: Experimental test conditions

Test Conditions	**Range**
Operation frequency of blower, f, Hz	10, 20, 30, 40, 50
Crossflow velocity, u, m/s	2.15 – 12.63
Supply pressure in feed water, P, bar	0.25, 0.5, 0.75, 1.0
Jet exit velocity, U_0, m/s	3.51 – 7.78
Liquid/gas density ratio, ρ_L / ρ_G	802.2

The relationship of the liquid jet velocity, liquid Reynolds number and the We number of cross flow air are presented in Table 4.

Table 4: Connection between the supply pressure in feed water and the jet exit velocity

Supply Pressure (bar)	**Jet Velocity (m/s)**	**Re_{liquid}**
0.25	3.51	1349
0.50	5.32	2046
0.75	6.60	2539
1.0	7.78	2993

As stated earlier the centrifugal fan was a frequency from inverter in order to rotate. The rotating velocity of blower is proportional to the frequency of the power supplied by the inverter, hence

the air stream velocity is proportional with the inverter frequency. Table 5 shows the correspondence between rotating frequency and the air stream velocity and responded aerodynamic Weber number.

Table 5: Correspondence between rotating frequency with cross flow velocity and aerodynamic Weber number

Frequency	**Cross-Flow Velocity (m/s)**	**We_{air}**
10	2.15	0.04
20	4.78	0.20
30	7.45	0.47
40	10.16	0.87
50	12.62	1.34

The parameters which describe the experimental process are Reynolds number (Re), aerodynamic Weber number (We), Ohnesorge number (Oh), liquid-to-air momentum ratio (q). The Reynolds and aerodynamic Weber number ranged from 1349 to 3036 and 87.9 to 445.1 respectively. The liquid to air momentum flux ratio ranging from 62 to 10814. In all cases, the Ohnesorge number was very small (Oh<0.0069), therefore the effect of viscosity is minimum. The parameters are also summarised in Table 6.

Table 6: Test parameters

Parameter	**Range**
Crossflow air Reynolds number, Re_g	14024 - 82319
Liquid jet Reynolds number, Re_L	1349 - 2993
Liquid jet aerodynamic Weber number, We_L	87.9 – 432.5
Crossflow aerodynamic Weber number, We_g	0.04 - 1.34
Air-to-liquid momentum flux ratio, q	$1x10^{-4}$ – $161x10^{-4}$
Ohnesorge number, Oh	< 0.0069

3.3 **Blower Calibration**

It is important to know the air flow velocity profile at the exit of the tube section. The velocity of cross flow influences the liquid jet trajectory and the way that it breaks up. Hence, blower calibration process was necessary to characterize the air stream, in terms of the cross flow air flow rate air velocities across the diameter of the tube exit. For the blower calibration a hot wire anemometer was employed to measure the air velocity. The hot wire was attached on a custom base which could move with high accuracy vertically across the tube diameter. Blower calibration was conducted for inverter frequencies between 5 and 50 Hz. The vertical centreline of

the tube was divided in twelve points with one centimetre distance between them and the air velocities were measured at each point for each considered blower speed. Consequently, the combination of all the collected data defines a cross flow air velocity profile for the exit of the tube. The air velocity profiles for the range of 5 to 50 Hz inverter frequencies are shown in Figure 3.1. Therefore, the boundary conditions of cross flow air are well defined.

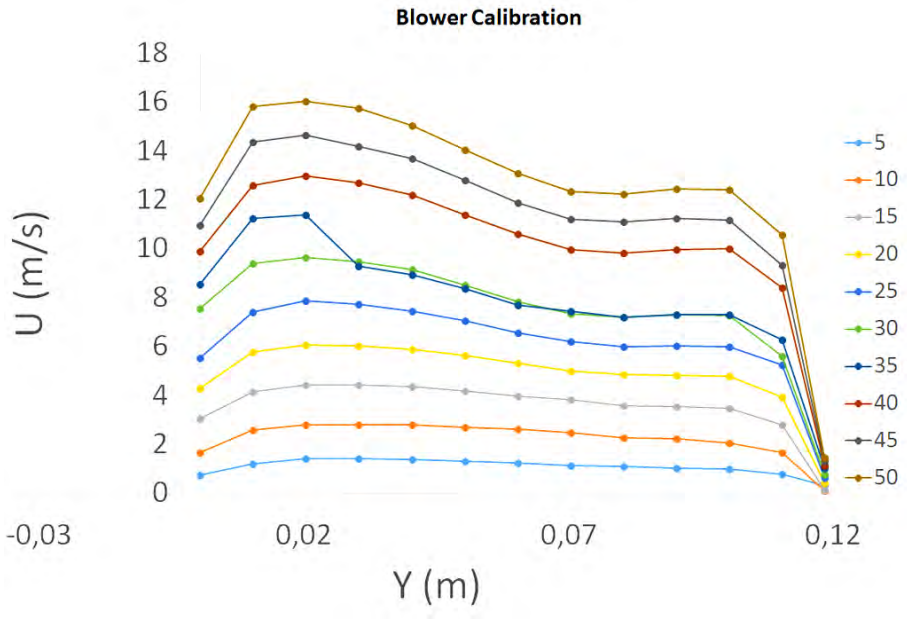

Figure 3.1: Blower calibration

Additionally, the mean volumetric flowrate was estimated for each blower operation frequency. For the calculation of flow volume, the cross section of the tube was divided in rings centred on the velocity measurement points. Then a mean flow volume for each frequency was calculated as the equation is shown:

$$Q = u_i * dA_i$$

The calculation results for mean flow volume in different inverter frequencies are presented in Table 7.

Table 7: Mean flow volume in different inverter frequencies

f (Hz)	5	10	15	20	25	30	35	40	45	50
Q (m^3/s)	0,011	0,023	0,037	0,052	0,066	0,081	0,088	0,111	0,124	0,138

3.4 Liquid Flow rate Calibration

Attention is given on liquid flow rate because different mass liquid flows are expected to effect the liquid jet penetration in the gas cross flow. When the inlet pressure changes the feed

water flow is modified, hence a range of different liquid flow volumes and liquid velocities are achieved. For the liquid flowrate calibration process, a high accuracy scale was employed in order to weigh the water mass that was injected from the nozzle at specific injection pressures which correspond to specific liquid jet velocities. The density of water is constant at ρ=999.7 Kg/m^3, the nozzle diameter is D_0=0.5 mm, and therefore the flow out surface of nozzle is A_{nozzle}=0.2mm^2. The calibration was conducted for injection pressures of 0.25, 0.5, 0.75, 1.0 bar and the injection duration was 120 seconds during which the injected water was collected. The collected water was then weighed on an electronic scale. The liquid flowrate calibration was carried out for the aforementioned pressures and was repeated three times in order to calculate a mean liquid mass flow rate for each pressure and ensure repeatability. After the liquid mass is measured the liquid volume is calculated from equation: $\rho = \frac{m_i}{V_i}$. The liquid flow rate is calculated from the division of liquid volume by the injection time: $Q_i = \frac{V_i}{t}$. Finally, the liquid velocity is calculated as: $U_{0i} = \frac{Q_i}{A_{nozzle}}$, namely, the liquid flow rate is divided by surface area of the nozzle exit

In the following diagram the relation between volume flow rate and the injection pressure in water is illustrated for the three measurements. It is worth noting that the three measurements of the flow rate are almost identical.

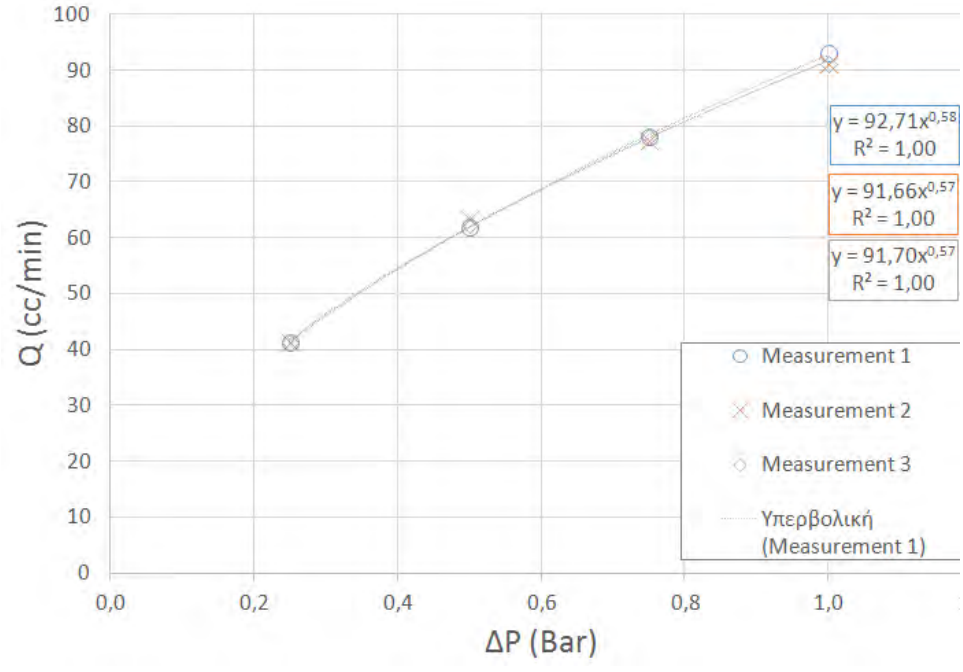

Figure 3.2: Liquid flow rate calibration

3.5 Camera Calibration

The camera placed across the atomizer in one meter distance for the experimental needs. Camera calibration is primary importance because shadowgraphy technique is based on large number of instantaneous images, that are essential to have a clear representation of liquid jet, to have an light illumination in background and the camera must be focus on jet surface. The camera which was employed for the experiments is appropriate for industrial environments, the resolution is 2592 × 1944 pixels with a maximum frame rate in 14 fps. Before we start recording, open the vimba software which is appropriate for the allied vision camera and where someone can change the camera calibration. The maximum frame rate is 14 fps but for these experiments the camera setting was in 4 images per second. The exposure channel was changed in value 10000 μs and the saved images were change in .tiff type. The camera device has two configurations, the first is the focusing and the second is the aperture Figure 3.3. The right combination of these two calibrations, send back an image with a perfect focus on surface jet and an appropriate illumination. Recorded images are saved in unique folder for each experimental measurement.

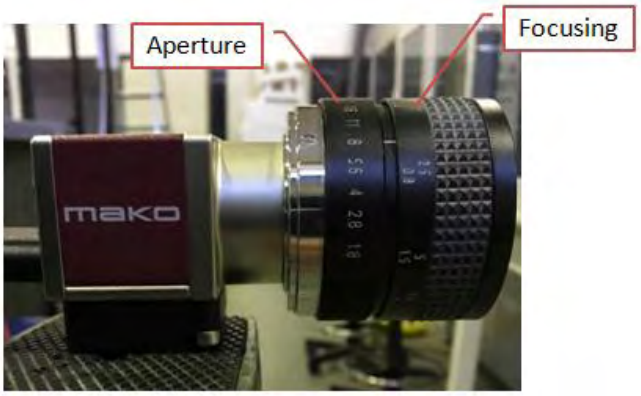

Figure 3.3: Camera calibration (Aperture, Focusing)

At the beginning of each experiment, a large number of backgrounds, without jet injection, are recorded in order to calculate a mean background that it will be used in image processing Figure 3.4 (a). Furthermore some images are taken with a vertical ruler near to nozzle, for a better calibration and for realistic representation of jet length and penetration length Figure 3.4 (b).

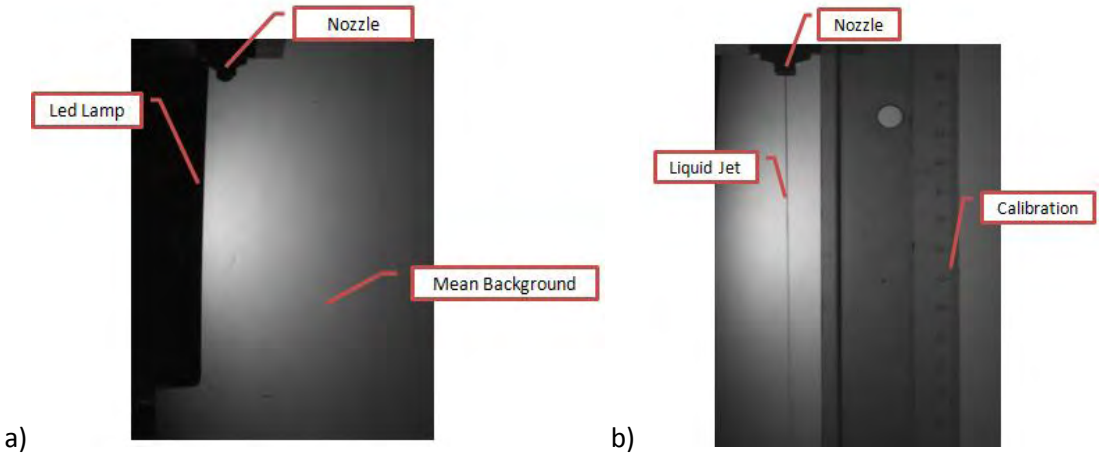

Figure 3.4: a) Mean background, b) Calibration

3.6 **Image Processing**

A large number of instant images were taken during the experimental measurements in order to characterize the liquid jet which was injected into a cross flow stream. The jet acquires a complex structure during the interaction with cross flow air as it is revealed through the images of shadowgraphy technique. Based on optical connectivity measurements and image processing, an algorithm was developed in Matlab in order to process various images. Matlab is appropriated for image processing because all the images are corresponded to a 2-D matrix, where each element of the formed matrix represents a pixel of the initial image with a specific value. It is of primary importance to determine the size of one pixel which corresponds in real size of one millimetre on a specific image. That comes through via image calibration with a ruler that gives a real sense of image size and actually we can calculate how many pixels equal millimetre. On this set of measurements we use a distance of 10 cm to calculate the corresponding pixels and then a ratio of millimetres via pixels (1000/pixels) is used in algorithm to convert the pixels values to millimetres.

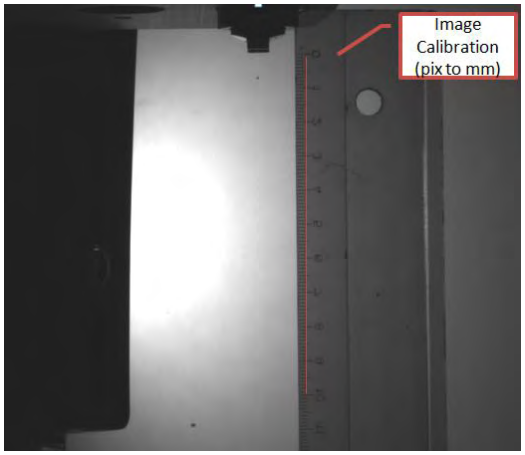

Figure 3.5: Image calibration

The existing algorithm is built to read a large number of instantaneous images (500 images) and processes the data from images, for each separated measurement case. Furthermore, a number of 40 images from background had been taken before the experiments started. A unique script algorithm processes these images from background in order to receive a mean background that is going to be used in main algorithm. Initially, the receiving images are monochrome with various values in matrix that indicates the light intensity Figure 3.6 (a). At the beginning of image processing, a general mean background, which has been taken Figure 3.6 (b) is removed from each monochrome images in order to isolate only the jet structure and remove any noise from images in Figure 3.6 (c).

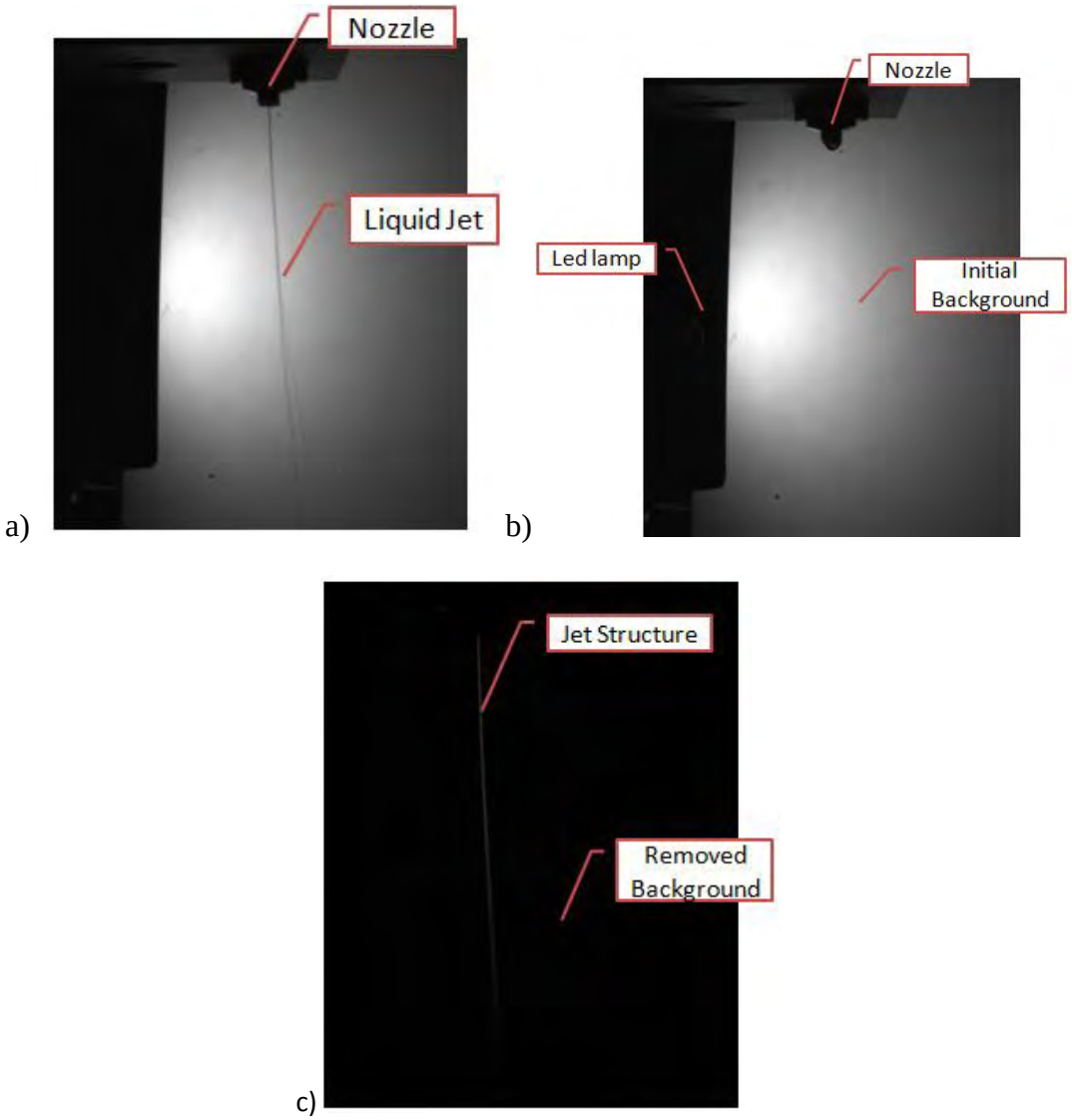

Figure 3.6: a) Initial monochrome image, b) Mean background, c) Jet structure isolation

The initial grayscale image without background is cropped in order to be moved the point from the exit of nozzle at the up and left corner of the image. Afterwards, a graythresh-filter for removing automatically the noise from grayscale is applied in order to convert the grayscale image into a binary form. Special attention must be given in filter level because in conditions with high crossflow velocity the liquid jet is oscillated and some ligaments, droplets are resulted from initial jet, therefore images have much more noise that must be removed with a high-filter level. Then the image is converted into a binary image where the zero value represents the black background and the one value indicates the light areas of image Figure 3.7. Primary breakup regime include only the jet form until the first point where the initial jet breakup in ligaments and other particles. These secondary areas which are smaller than the jet area and hence have lower boundaries than the higher jet boundaries are removed from the binary image in order to remove the further noise and to remain only the jet structure until the first breakup point Figure 3.8.

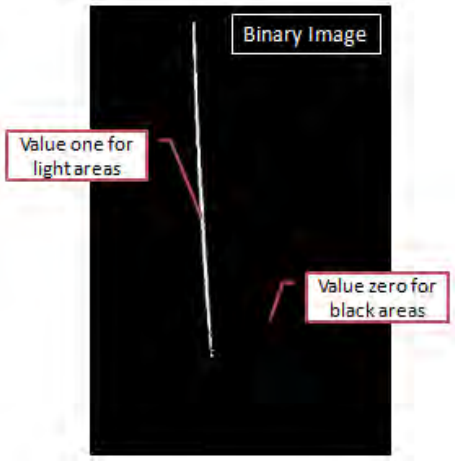

Figure 3.7: Binary Image

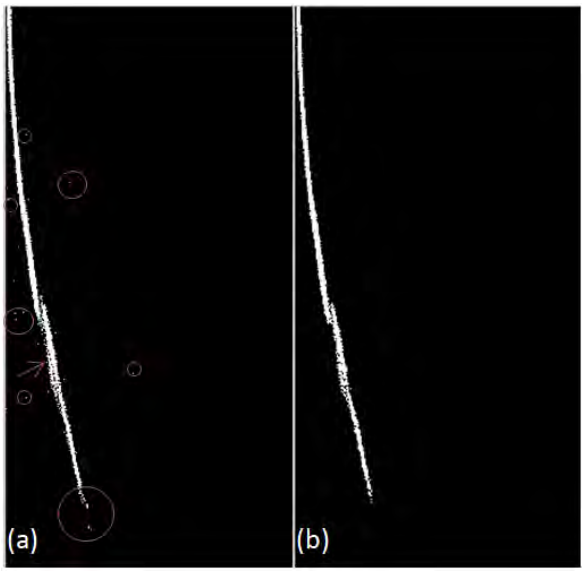

Figure 3.8: Remove noise and areas with low boundaries

Below in algorithm a special command find the non- zero values from binary image and hence we achieve a matrix with jet coordinates in pixels. The pixels coordinates are multiplied with the value from image calibration and are converted into millimetres coordinates. In an attempt to define the jet trajectories is was necessary to find a curve that is fitted on the centreline of jet form with a starting point being the exit of the nozzle and an ending point being the first break up spot which is the last continuous pixel with value one. Plotting the coordinates that consist the centreline arise a curve similar with a 2nd degree polynomial curve. In order to calculate the trajectory of each instantaneous image is essential to fit the centreline of jet with a unique 2nd degree polynomial curve and for this reason we calculate the coefficients of polynomial and then we plot a curve that is fitted to begin from (0,0) coordinates. This calculate is verified with plotting at the same time both of curves. From the previous image processing and with

appropriate algorithm we can define the penetration length of each instantaneous trajectory and also the entire length of jet bulk until the first break up position. For the length measurements used the subtraction between two points and more specifically between the coordinates (x, y). For each of 500 repetitions all the results and the parameters are saved in vectors and matrixes. At the end of image processing values such as penetration length, total length of jet, the coefficients values of polynomial are collected in a general matrix unique for each experimental measurement. During image processing of 500 images the parameters of penetration length and jet length are saved in vectors in order to calculate a mean value of these parameters for each measurement. Below the mean values will be compared with each other in the following results. Furthermore, the typical jet trajectory can be represented from a power law functional relationship between x and y jet coordinates ($y = bx^m$). For that reason the dynamic power law function is fitted with the centerline of jet and the coefficient (b, m) for each curve are saved in order to calculate a mean power law curve. Additionally, algorithm calculate the standard deviation of x coordinates from a mean x-value at the same y coordinate and the mean absolute error of power law curve from the typical experimental jet curve. All the above results of each case are saved, at the end of algorithm, in excel files.

3.7 Statistical Analysis Methods

3.7.1 Mean Absolute Error (MAE)

Mean absolute error (MEA) is one of the most common metrics methods in statistics to calculate the accuracy of continuous variables. This method is used to measure the average size of the errors in a set of actual observation that apply to the same phenomenon.

$$\mathrm{MAE} = \frac{1}{\mathrm{n}}\sum_{\mathrm{j}=1}^{\mathrm{n}} |\mathrm{y_j} - \bar{\mathrm{y}}_\mathrm{j}|$$

In the present study mean absolute error method is employed to measure the average distance between each point of the experimental trajectory in x-coordinates and the power law curve. The scope of this calculation is to observe the amount of deviation from the power law curves that represent a dynamic curve which fits with the experimental trajectories of jet. MAE shows the accuracy of fitting the power law model with the actual points of jet. Furthermore, in this way we can investigate and compare the deviation from the real jet trajectory at the beginning and at the bottom of jet.

3.7.2 Standard Deviation

Standard deviation is a method of measurement that is used to quantify the amount of dispersion of a set of data values. It is calculated as the square root of variability by determining the variation between each data point relative to the expected value. A low standard deviation indicates that the data points tend to be close to the expected value of the set, while a high standard deviation indicates that the data points are spread out over a wider range of values (https://en.wikipedia.org/wiki/Standard_deviation). The formula of standard deviation is shown below:

$$s = \sqrt{\frac{\sum_{j=1}^{n}(x_j - \bar{x})^2}{n-1}}$$

In current study standard deviation calculation give the variation between actual x values of jet trajectory and mean values of all x values for each y value. Both of the developed statistical procedures help us to understand the behaviour of jet and how wide is the divergence in each instance.

4. Results and Discussion

4.1 Mean Jet Profile Trajectories

In this chapter the results of the experimental sets are presented and are compared. The entire experimental process consists of 20 different cases which have been occurred from the combination of the 5 different crossflow velocities and 4 dissimilar supplied liquid velocities. The round non-turbulent water jet behaves differently under the various flow conditions, hence the following results describe this behaviour in each set of experiments. Firstly, the mean jet profile trajectories are presented at specific Reynolds number as a function of aerodynamic Weber number of cross-flow air. On diagram illustration, all the jet trajectories profile begin from point (0,0) that represents the nozzle exit. The y-axis is aligned with the direction of injection, whereas the x-axis is aligned with the direction of the air cross-flow. Aim of this investigation is to analysis the collecting data in order to calculate a mean jet trajectory for each of 20 different experimental cases. Additionally, the jet trajectories are fit to power law functions which can supply a mathematical expression of the trajectories.

4.1.1 Jet Trajectories for Specific Reynolds Numbers

1st Experimental Set for Re=1349 and We=0.04, 0.20, 0.47, 0.87, 1.34

First of experimental measurements have been carried out at steady water supply pressure at 0.25 bar which corresponds to about 3.5m/s jet exit velocity and also flow rate Q=41.33cc/min. At these conditions the Reynolds number is Re=1349 and the round liquid jet a non-turbulent. The blower driving frequency ranged from 10 Hz to 50 Hz and the cross flow air velocities produced are proportional with mean value from 2.15 m/s to 12.62 m/s. These gas flow velocities are described from the aerodynamic Weber number of We=0.04, 0.20, 0.47, 0.87, 1.34. In the following diagram are illustrated the mean jets profiles in x, y coordinates for constant Re=1349 as they occur from the data processing Figure 4.1 **Σφάλμα! Το αρχείο προέλευσης της αναφοράς δεν βρέθηκε.**. The trajectories curves are a function of the liquid Reynolds number and aerodynamic Weber numbers. With thick continuous curves are illustrated the mean jet trajectories and the light-colored discontinuous curves represent the fitting of power law function in jet trajectories. This experimental set is the most weak among the other sets because has the lowest Reynolds number and as a consequence the highest air to liquid flux momentum ratio ($5*10^{-4}< q <161*10^{-4}$), hence the jet entrain easy from cross-flow trajectories. Moreover, strong disturbances occur at the breakup area of jet and that create noise. The noise is illustrated at the

edge of the trajectories where the curve appears to be dislocated. The experimental results show that at constant liquid Reynolds number the minimum incline appear at the lowest gas Weber number and as the Weber number is increased the incline of trajectories become more steep. As we stated earlier, the light-colored discontinuous curves represent the fitting of power law function in existing jet trajectories. Generally, the power law curve follows almost the same trajectory with the experimental jet trajectories and it means that this mathematical function describes with high accuracy the jet trajectories in cross flow conditions. However, the fit for the case of Re=1349 and the most powerful We=1.34 deviate substantially from jet trajectory and hence the fitting is wrong in this case. That happens due to the powerful disturbances on the liquid jet and the irregular trajectories that follow the jet in these conditions.

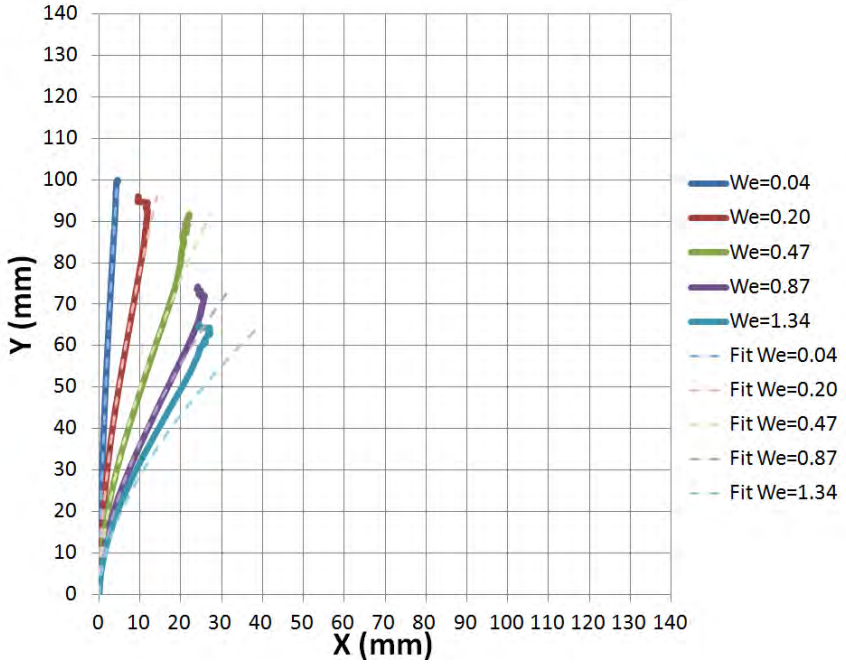

Figure 4.1: Mean jet profiles for liquid Re= 1349 and We=0.04, 0.20, 0.47, 0.87, 1.34

2nd Experimental Set for Re=2046 and We=0.04, 0.20, 0.47, 0.87, 1.34

A small modification in feed water pressure at P=0.50 bar, has as a result to increase the jet exit velocity at 5.32 m/s and also the flow rate at Q=62.66 cc/min. The liquid Reynolds number develop into Re=2046. Consequently, the momentum of liquid bulk become higher and the liquid jet resist further in changes of trajectory from cross flow stream Figure 4.2. Now the trajectories of jets tend to be more close by the vertical axis than the previous set with the lower Reynold number which curves tend to diverge from the vertical direction. Furthermore, large values of Weber number influence much more the incline of jet trajectories and create larger disturbances at break up point, but smaller than the existed noise in trajectories of the previous

set. As the fitting of power law function has already been refered, we observe that the current results of fitting have been enhanced and the mathematical curves coincide with the experimental jet profile trajectories, except for the case Re=2046 and We=1.34 in which curve deviates slightly from the jet trajectory.

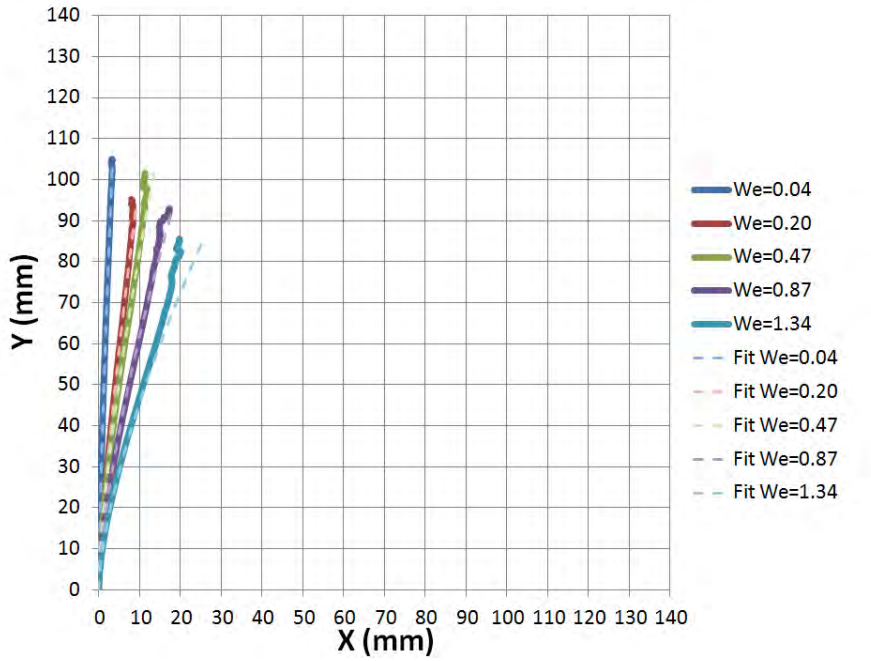

Figure 4.2: Mean jets profiles for liquid Re= 2046 and We=0.04, 0.20, 0.47, 0.87, 1.34

3rd Experimental Set for Re=2539 and We=0.04, 0.20, 0.47, 0.87, 1.34

For this set of experiments water is employed at P=0.75 bar supply pressure. This value of pressure changes the liquid flow rate into Q=77.79 cc/min and the corresponded jet velocity is U0=6.60 m/s. The new Reynolds value is Re=2539 and the liquid jet remain non-turbulence and at the same time the liquid momentum becomes more powerful. The air to liquid momentum ratio is still insignificant in this set and ranges at low values 1*10-4< q <46*10-4. In current experimental set the jet trajectories profiles for different conditions of aerodynamic Weber are very close to each other and tend to deviate the least from the vertical axis. These powerful liquid jets can't entrain easy from the air cross-flow and hence their characteristic trajectories are huddled very close among them and have a low value of gradient. Furthermore, the noise at the edge of trajectories has almost disappeared for all cases except for the case of Re=2539 and We=1.34 where a little noise still remains. In general, the functional power law curve is fitting exactly on the experimental trajectories with only a small deviation at the last case.

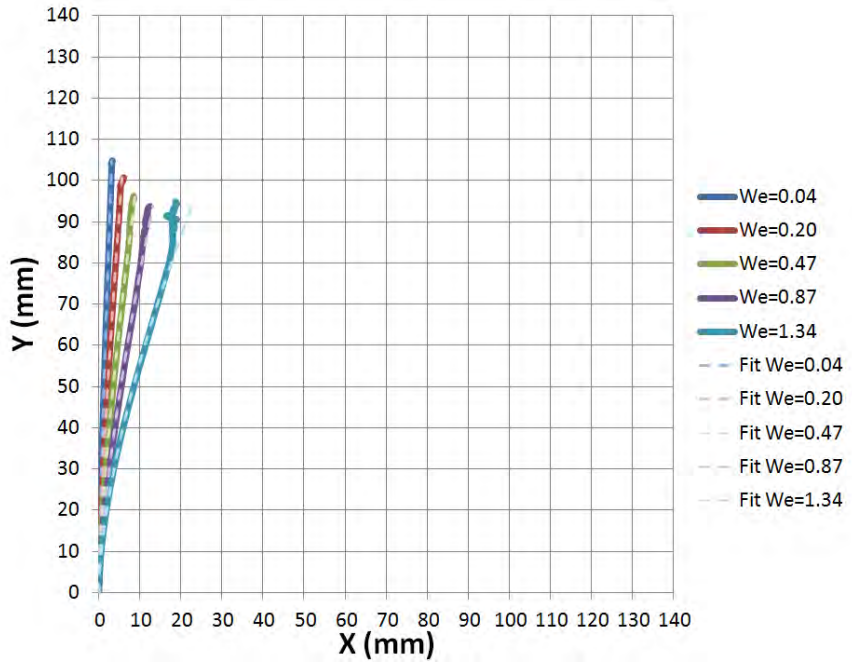

Figure 4.3: Mean jets profiles for liquid Re= 2539 and We=0.04, 0.20, 0.47, 0.87, 1.34

4th Experimental Set for Re=2993 and We=0.04, 0.20, 0.47, 0.87, 1.34

Finally, we supply at the nozzle water at pressure P=1.0 bar and the flow rate turns into at a much more higher value Q=91.67 cc/min. The existed jet velocity for these conditions is U_0=7.78 m/s and the Reynolds number receive the highest value for this experimental study at Re=2993. In the present set of experiments the liquid momentum is very high comparatively to the cross-flow air momentum, as the very low values of air to liquid flux momentum ratio demonstrate 1*10-4< q <33*10-4. Therefore the injected liquids tend to follow their initial trajectories and diverge very little from the vertical direction. Now we observe that for all different Weber cases, the trajectories are concentrated on one next to the other and follow similar trajectories with small values of grandniece, even at the most powerful cases with aerodynamic Weber (We=0.87, 1.34) Figure 4.4. The experimental trajectories touch exactly with the functional power law curve that is exposed from the data processing. Consequently, the dynamic power law curve fits with high accuracy with the experimental results for the jet trajectories and we can say that it is a mathematical expression which describes perfectly the jet trajectories behaviour.

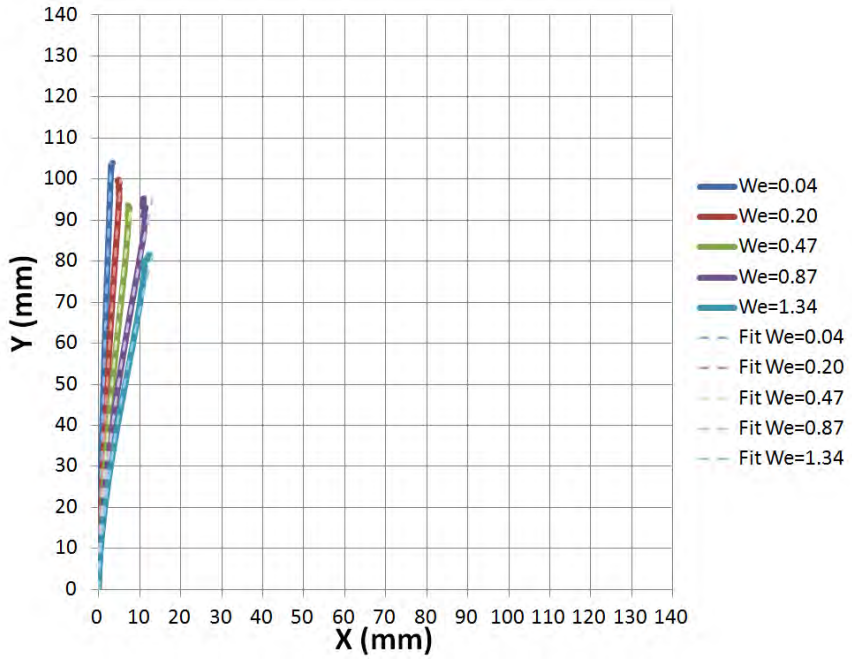

Figure 4.4: Mean jets profiles for liquid Re= 2993 and We=0.04, 0.20, 0.47, 0.87, 1.34

A summary of the coefficients of the power law is represented below. Obviously, in different liquid Reynolds numbers and different aerodynamic Weber numbers the power law curves follow dissimilar trajectories with dissimilar coefficients of the functional expression. As we said earlier, the functional power law equation is: $y = b * x^m$ and the coefficients are the value b and the exponential value m. In Figure 4.5 are illustrated the values of the coefficient b in different Weber numbers for the four different liquid Reynolds number. Whereas, in Figure 4.6 are illustrated the values of the exponential coefficient m depending in Weber number for the different liquid Reynolds numbers.

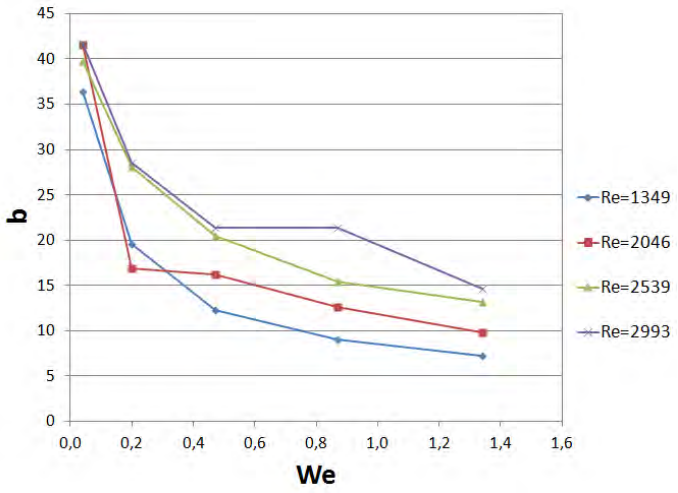

Figure 4.5 : Values of b coefficient for Re=1349, 2046, 2539, 2993 and We=0.04, 0.20, 0.47, 0.87, 1.34

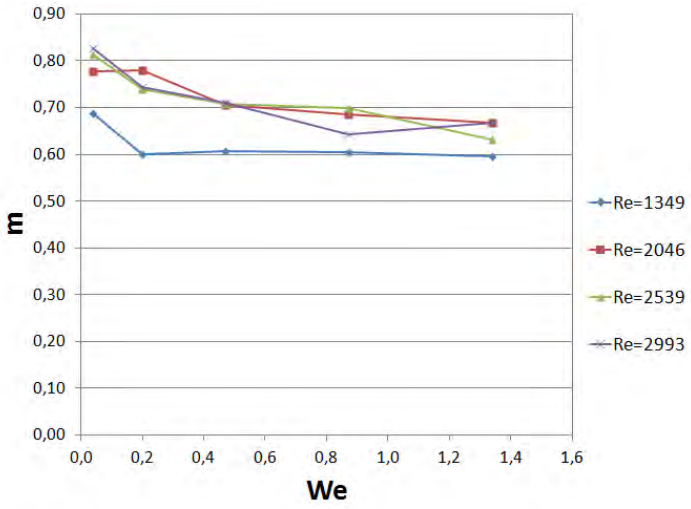

Figure 4.6: Values of m exponential coefficient for Re=1349, 2046, 2539, 2993 and We=0.04, 0.20, 0.47, 0.87, 1.34

4.1.2 Jet Trajectories for Specific Aerodynamic Weber Numbers

In order to observe better the results of experimental jet trajectories for each cross-flow air conditions, we plot on graphs the characteristic jet trajectories for a unique aerodynamic Weber number and for different Reynolds numbers, as a function between x and y coordinates Figure 4.7. The following five diagrams correspond to the five dissimilar cross flow conditions with their characteristic Weber number. More analytically, for the first set of experiments the blower rotation frequency is 10 Hz that produces a mean cross-flow velocity u=2.15 m/s and a Weber number about We=0.04 Figure 4.7 (a). Subsequently a gradually increase of inverter frequency has as a result to raise the cross-flow air velocity at u=4.78, 7.45, 10.16, 12.62 m/s and the Weber number turns into We=0.20, 0.47, 0.87, 1.34 correspondingly Figure 4.7 (b), (c), (d), (e). At low Weber numbers the jet trajectories coincide and they are almost one above the other We=0.04, 0.20. Increasing the cross flow air velocity and the We at the same time, then the liquid jet entrains easier from gas stream, as it is illustrated in the diagrams below. Among all cases the most remote jet trajectory is this with the lowest Reynolds number Re= 1349, namely with the highest air to liquid flux momentum ratio 33*10-4< q <161*10-4. Furthermore in the last experimental sets with high Weber We=0.87, 1.34 some noise is produced at the jet trajectories.

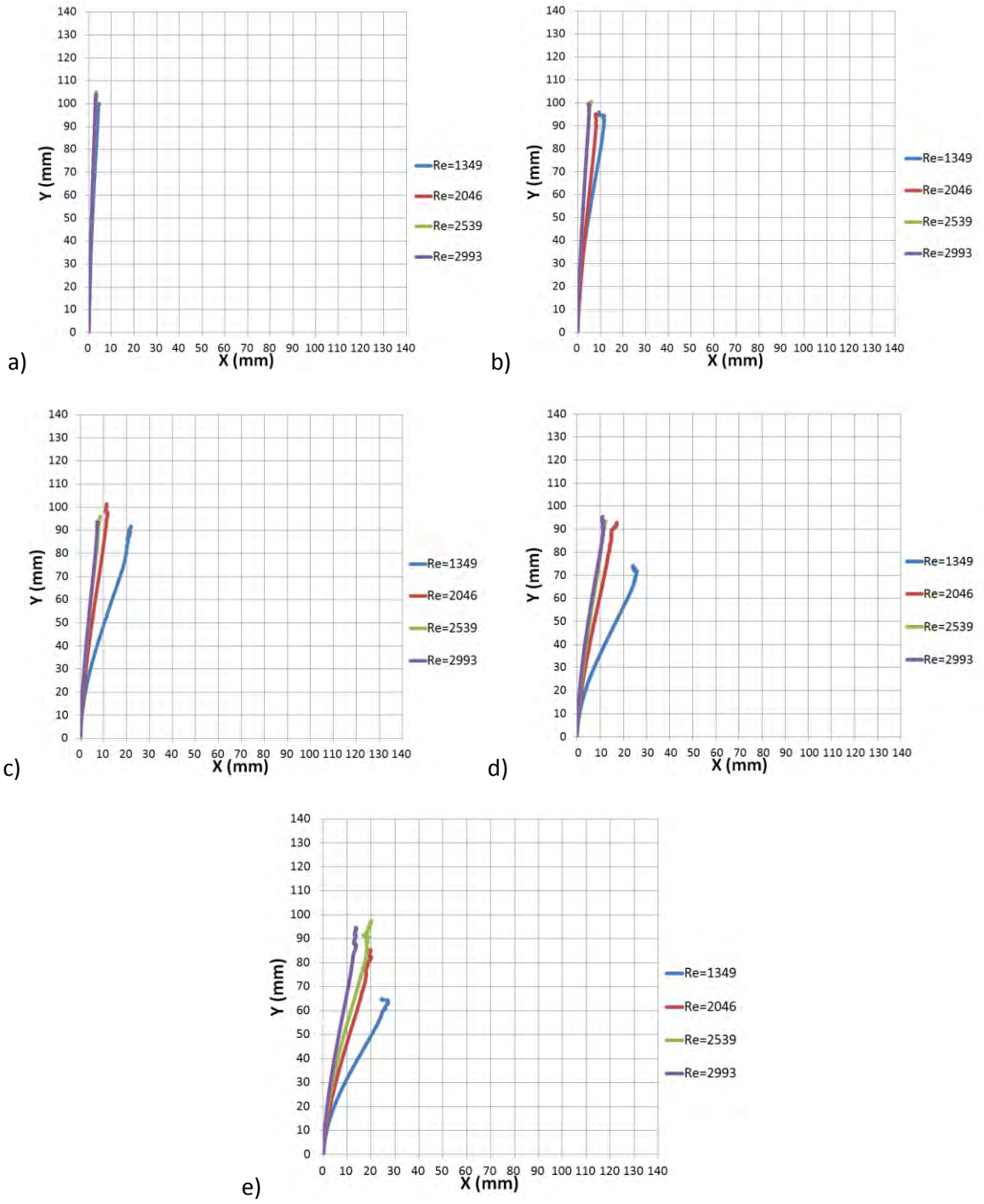

Figure 4.7: Jet trajectories for specific aerodynamic Weber numbers a)We=0.04, b)We=0.20, c)We=0.47, d)We=0.87, e)We=1.34 for Reynolds Re=1349, 2046, 2539, 2993

4.2 Characteristics of Jet Formation

As we discussed earlier, in this study we focus on primary break up process of the liquid jet. In an attempt to characterize better the structure of jet it is important to mention some basic geometric characteristics of the round non turbulence jet formation. Therefore, in present investigation we consider the primary penetration length of jet, also the penetration along the gas

flow axis and the total length of liquid jet until the first breakup. In general, these parameters lead us to a better understanding of jet spatial formation in different conditions. After the image processing and data analysis some values have arisen as far as penetration length, penetration along the flow axis and total length in various test conditions are concerned. The results gathered from these parameters for each dataset of measurement are of great interest. In the following paragraphs there is an analytical description of the foregoing parameters.

4.2.1 Penetration Length & Penetration along Flow Axis

The term penetration length in primary breakup is defined by the vertical distance from the exit of nozzle until the first breakup point of liquid jet Figure 4.8. This value shows the exact length that the jet penetrates into the air flow stream until the first break up and is proportional to the Reynolds number of the liquid, the aerodynamic Weber number and the liquid to air momentum ratio of jet. The horizontal distance from the exit of nozzle until the jets first breakup point is referred to as the penetration along the air flow axis Figure 4.8. Respectively, this value describes how long the jet penetrates along the gas flow axis and is modified in relation to Reynolds, Weber number and liquid to air momentum ratio.

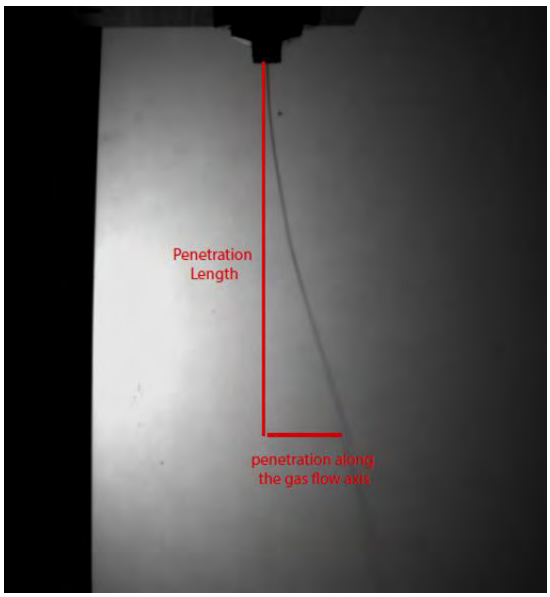

Figure 4.8: Penetration length and penetration along flow axis

The existed algorithm in matlab calculates the penetration length of each of 500 images and then calculate a mean penetration length of jet for each experimental case. In Table 8 the values of penetration length for combination of different liquid Reynolds number of liquid jet and aerodynamic Weber number of cross flow air are summarized. The maximum value of all experimental cases, is 98.4 mm distance and corresponds to the highest Reynold number of liquid and to the lowest aerodynamic Weber number, that is a logical outcome because the air to liquid

momentum ratio is very low and the liquid jet penetrates further. In contrast, the minimum value is the 42.5 mm penetration length which refers to the lowest Reynolds number and highest Weber number, namely to the highest cross flow velocity that cause for the earliest break up. In this combination of conditions the jet can not grow too much, as a result to breakup early and not to penetrate further into the gas cross flow. In general, for a constant value of liquid flowrate and so constant value of Reynolds number, as the cross flow air velocity is increased (We increased) so the penetration length is decreased. This phenomenon of jet penetration in cross flow is shown in Figure 4.9.

Table 8: Mean penetration length for each case

Re / We	0.04	0.20	0.47	0.87	1.34
1349	95.1	81.1	71.7	57.6	42.8
2046	97.9	81.7	80.1	71.2	61.1
2539	98.1	91.8	84.4	79.3	74.0
2993	98.4	92.3	83.3	77.7	63.6

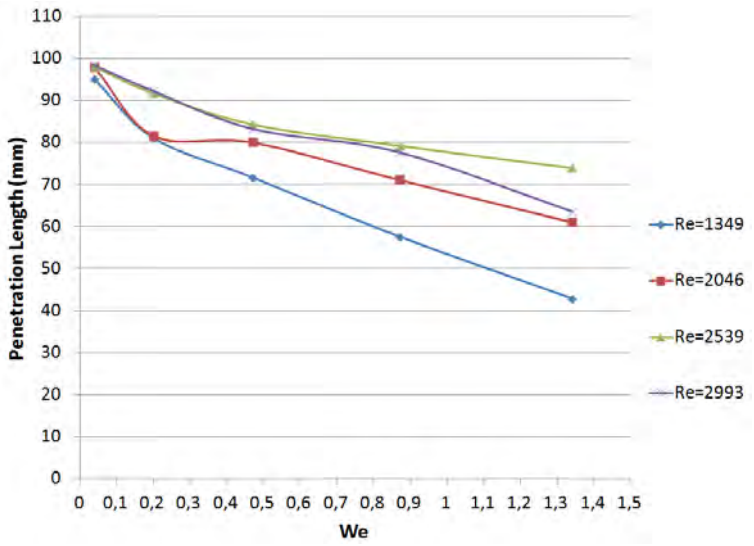

Figure 4.9: Jet penetration length in cross flow for Re=1349, 2046, 2539, 2993 and We=0.04, 0.20, 0.47, 0.87, 1.34

As the cross flow volume flowing along the horizontal direction entrain the vertical liquid jet. Hence, the jet penetrates along the gas stream axis, as a result to deviate from the vertical axis. The penetration along the gas flow axis is defined by the distance on the horizontal axis between the exit of the nozzle and the first break up point of the jet. It is obvious that higher cross flow velocities entrain easier a liquid bulk with standard liquid flow rate. Furthermore, the liquid jets with high air to liquid momentum ratio can't resist to the change of their direction and entrain easily from the air flow. In these sets of experiments the maximum penetration along the gas flow axis is the value 20.7 mm that correspond to the lowest liquid Reynolds number and for the

Weber number with the value We=0.87, whereas the minimum value is 2.7 mm for case with the lowest We and the highest Re, Table 9, something that was expected. It is interesting that for jets with Re=1349, 2993 for the highest value of Weber number, that means for the highest cross-flow velocity, the value of penetration in flow axis is lower than the previous value in We=0.87. That happens because in these conditions with the highest cross flow velocity the jet breaks up earlier and as a result it doesn't grow further along to the flow axis. Whereas a different behaviour is observed in cases with Re=2046, 2539 where the penetration is increased gradually and the We number is not enough to disintegrate the jet earlier Figure 4.10.

Table 9: Penetration along the gas flow axis

Re / We	0.04	0.20	0.47	0.87	1.34
1349	4.0	10.6	17.8	20.7	16.8
2046	3.0	7.5	10.0	12.3	13.6
2539	2.9	5.0	7.4	10.3	14.3
2993	2.7	4.9	6.7	9.4	8.9

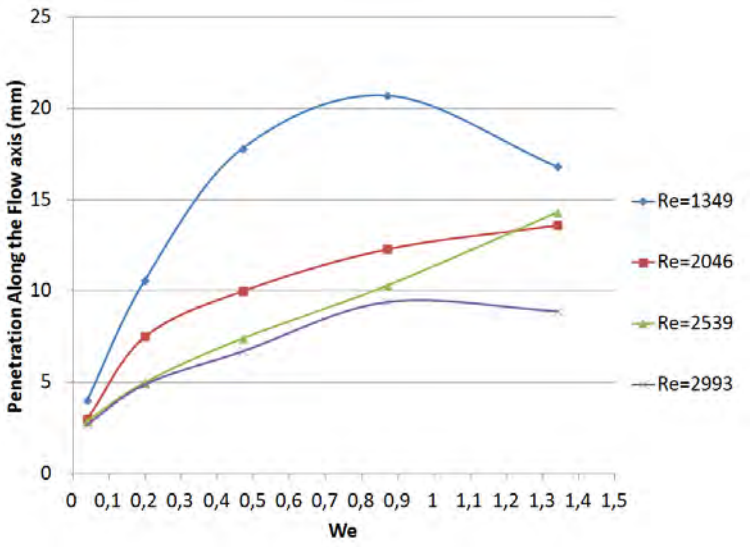

Figure 4.10: Penetration along the gas flow axis for Re=1349, 2046, 2539, 2993 and We=0.04, 0.20, 0.47, 0.87, 1.34

4.2.2 Primary Breakup Length of Liquid Jet

One of the most important characteristics of jet structure is the total length until the first breakup. This length is referred to as primary break up length and it is the initial liquid core, which disintegrates in the following phases of atomization of the liquid jet. The primary breakup length of a round non-turbulence jet depends on the liquid Reynolds, the air to liquid momentum ratio and also on the aerodynamic Weber number of cross flow. Hence, so the liquid flow rate as

the cross flow air volume play an important role to the jet length formation. Among the experimental measurements the highest length value is 147.3 mm while the lowest value is 93.9 mm Table 10. For the case of Re=1349 the jet length is increased progressively with the We increase until a specific value and then the length become smaller. As the Weber number is increased, the liquid jet is disintegrated more rapidly. Consequently, the jet breaks up soon and near the exit of nozzle, so the total length is becomes gradually shorter. This behaviour approximately follows the liquid jet with Re=2046, while in the case of Re=2993, the length of jet is decreased gradually with the increase of We number Figure 4.11.

Table 10: Primary breakup length of liquid jet for each case

Re / We	0.04	0.20	0.47	0.87	1.34
1349	111.7	113.4	126.8	109.5	93.9
2046	118.2	121.3	125.8	123.5	122.2
2539	124.4	123.0	124.8	130.1	147.3
2993	124.0	115.0	111.7	111.5	103.4

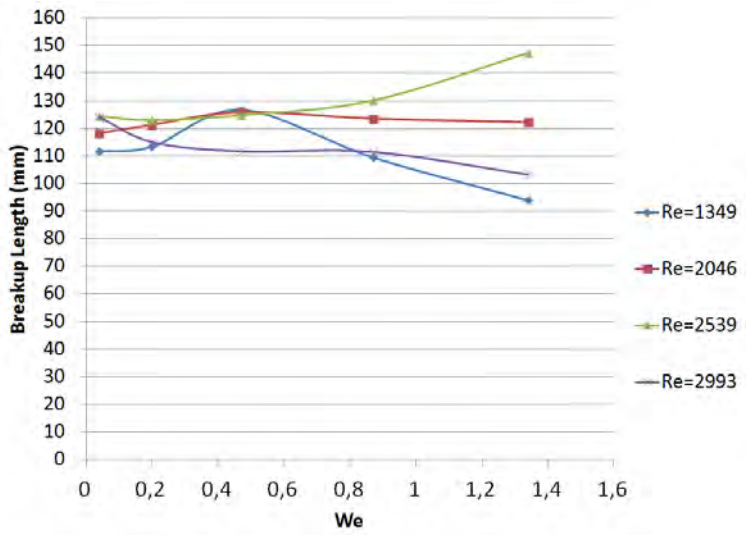

Figure 4.11: Primary break up length of liquid jet for Re=1349, 2046, 2539, 2993 and We=0.04, 0.20, 0.47, 0.87, 1.34

4.3 **Statistical Analysis Procedure**

It is of primary importance to take into account the probability of error in an experimental process. Therefore some statistical procedures have been employed for many investigators in order to describe the accuracy of their results or to infer conclusions for their experiments. A statistical analysis is significant for the correctness of the investigation results. During an experimental process the values in the same measurement set usually differ from each other or the

values of the same parameters vary. Hence, we have to consider the errors that result from deviations between the values. Large errors and deviation can sometimes lead on to incorrect conclusions. In present study we employed two statistical procedures for the analysis and verification of results accuracy. The employed statistical methods are the mean absolute error and the standard deviation analysis and both of them are presented in the following paragraphs.

4.3.1 Mean Absolute Error (MAE) Analysis

As we discussed earlier, a power law function is used to fit the experimental trajectories which resulted from the measurements. This functional model of curve is employed to describe the jet trajectories which seem to follow the dynamical process of jet development. Due to strong disturbances on the liquid jet and the disintegrated structures such ligaments and droplets, the fitting of the functional power law curve with the initial experimental trajectories has various deviances among them. In general, it has been proved in foregoing discussion that the employed power law functional relationship between the vertical y-coordinates and the horizontal x-coordinates of jet fit closely to the profile of trajectories. However, there is a deviation between the points of the trajectory and the fitting power law curve. Therefore, we investigate the mean absolute error between the real points of trajectory and the fitting curve in order to define the accuracy of power law model. In the following diagrams the mean absolute is presented error as a function of jet development downstream in vertical y-axis Figure 4.12. Each of four diagrams is for a specific Reynolds number (Re=1349, 2046, 2539, 2993) in different cross-flow condition (We=0.04, 0.20, 0.47, 0.87, 1.34).

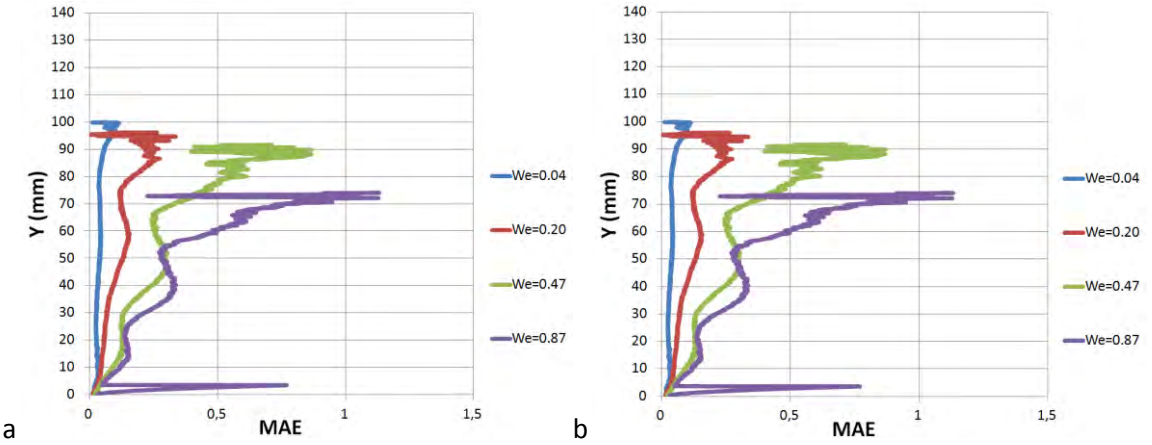

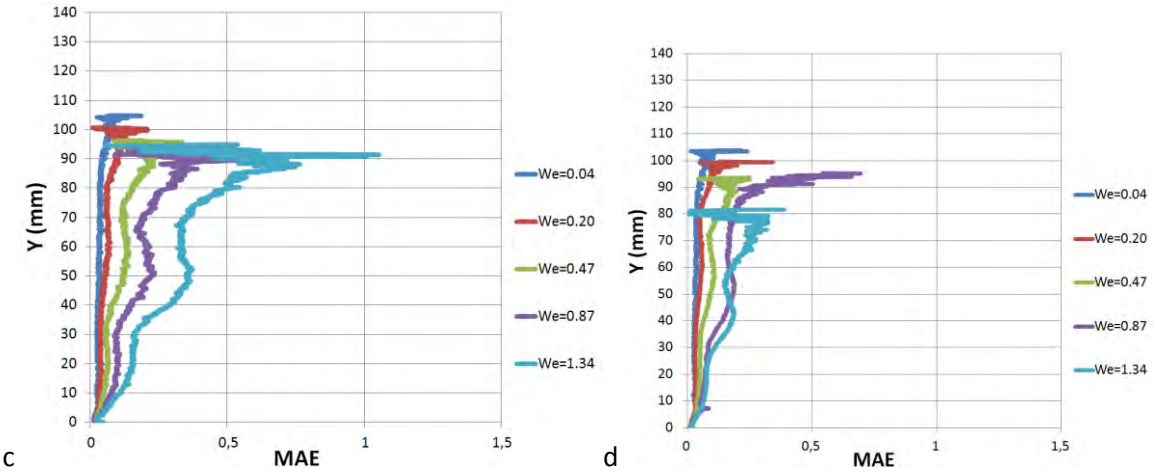

Figure 4.12: mean absolute error between power law fitting and experimental trajectories for a) Re=1349, b) Re=2046, c) Re=2539, d) Re=2993

A general observation of the results of mean absolute error is that in low Reynolds numbers and low liquid momentum, the errors are increased continuously with the increase of cross-flow velocity and as a consequence with the increase of aerodynamic Weber number. That happens because higher Weber number provides stronger disturbances in jet formation and as a result the errors are increased. Furthermore, higher values of errors are observed at the edge of where the breakup occurs and the noise from disturbances is higher than in the area which is near the nozzle exit. Taking into account the increase of Reynolds, we can perceive from diagrams that as the Reynolds is increased then the air to liquid momentum ratio is decreased, hence the mean absolute errors are limited Figure 4.12 (d). Generally, the possibility of the occurrence of error is small with a proximate value MAE< 0.5 mm and the results are accepted, besides the cases with low Re=1349, 2046 and the highest We=1.34 Figure 4.12 (a), (b) ,where the mean errors are extremely large and as a consequence the fitting of power law is considered to be incorrect for these cases. Therefore, we can say that the power law functional curve fits very closely to the experimental trajectories with a low range of errors.

4.3.2 Standard Deviation Analysis of Points in Jet Trajectory

This statistical analysis was employed in order to observe the deviation between the points of the mean trajectory profile in a unique experimental set and the points of the experimental trajectories of all measurements of the set. Standard deviation value indicates the dispersion of the x-coordinates of an experimental trajectory, downstream the jet formation, from a mean x-coordinate value of a mean trajectory profile of the whole measurement and a unique y-coordinate downstream the mean jet trajectory. Actually, in this way we can investigate how much the data points tend to approach a specific mean value. Obviously the range of standard

deviation value depends on experimental conditions and how long the jet penetrates into cross-flow air stream. Further penetration in crossflow means stronger disturbances and higher oscillations on jet surface, as a result it follows that the data values deviate much more from the mean value than the data points which exist near the exit of nozzle. This result is confirmed from the diagrams in Figure 4.13. We observe that at the same time of the downstream jet development the deviations acquired higher values and specifically close to at the breakup area the deviation between mean value and experimental points of trajectory receive the highest value. Consequently, stronger disturbances near the breakup area, leads to higher standard deviation values. Additionally, the diagrams show that powerful liquid jet with higher jet velocities and higher Reynolds number introduce lower standard deviations than the cases with lower Reynold number. For the most weak experimental set for Re=1349, as the Weber is increased the air to liquid momentum ratio is increased too, hence high values of standard deviations are observed Figure 4.13 (a). However the maximum standard deviation value is about 3.5 mm from the mean value of the case Re=1349 and We=1.34.

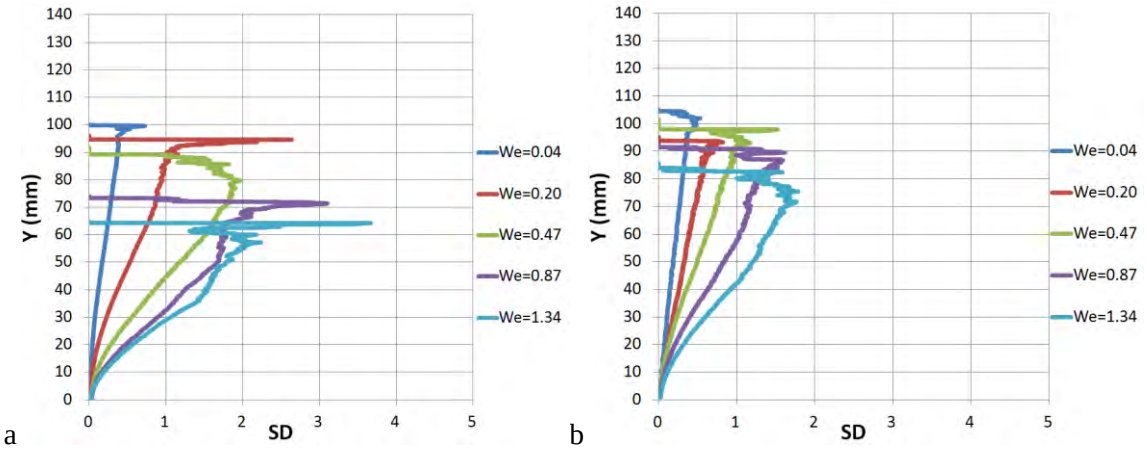

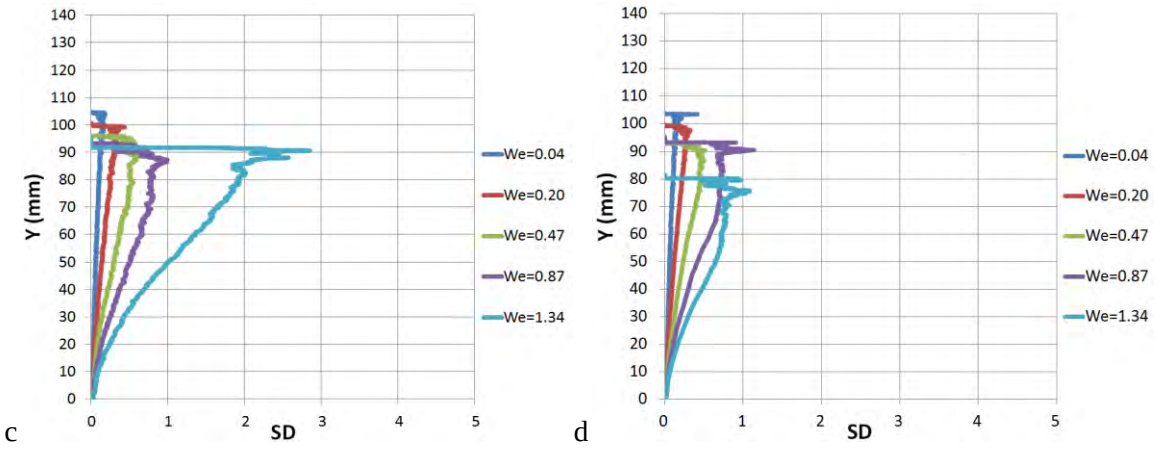

Figure 4.13: Standard deviation in jet trajectories for a) Re=1349, b) Re=2046, c) Re=2539, d) Re=2993 and We=0.04, 0.20, 0.47, 0.87, 1.34

4.3.3 Probability of Jet Presence

As the liquid jet penetrates into the cross-flow the aerodynamic forces, which act on the surface, disintegrate the jet into ligaments and droplets. Depending on parameters such as liquid Reynolds number, the aerodynamic Weber number and air to liquid flux momentum ratio, the liquid jet disintegrates in different point in relation with the experimental conditions of each case. For this reason special attention is given to the probability of jet presence downstream to the jet formation. Hence, a rate that defines exactly the percentage of jet presence along the vertical jet axis is employed. These percentages are illustrated in the following diagrams Figure 4.14. The rate of 100% determines the indisputable presence of liquid jet in a specific distance from the exit of nozzle. In general, as the liquid jet moves away from the exit of nozzle then the percentage of jet presence is gradually decreased. In low Reynolds cases the rate of jet existence is decreased in shorter distance from the exit nozzle than the higher Reynolds cases which penetrate further downstream the jet. Moreover the cases with low aerodynamic Weber number We=0.04 have the strongest presence along the jet. We must point out that the cases Re=1349, We=1.34 and Re=2046, We=1.34 with air to liquid momentum ratio $q=161*10^{-4}$, $70*10^{-4}$ are illustrated wrongly in diagrams Figure 4.14 (a), (b) due to some wrong results because of strong disturbances and rapid disintegration.

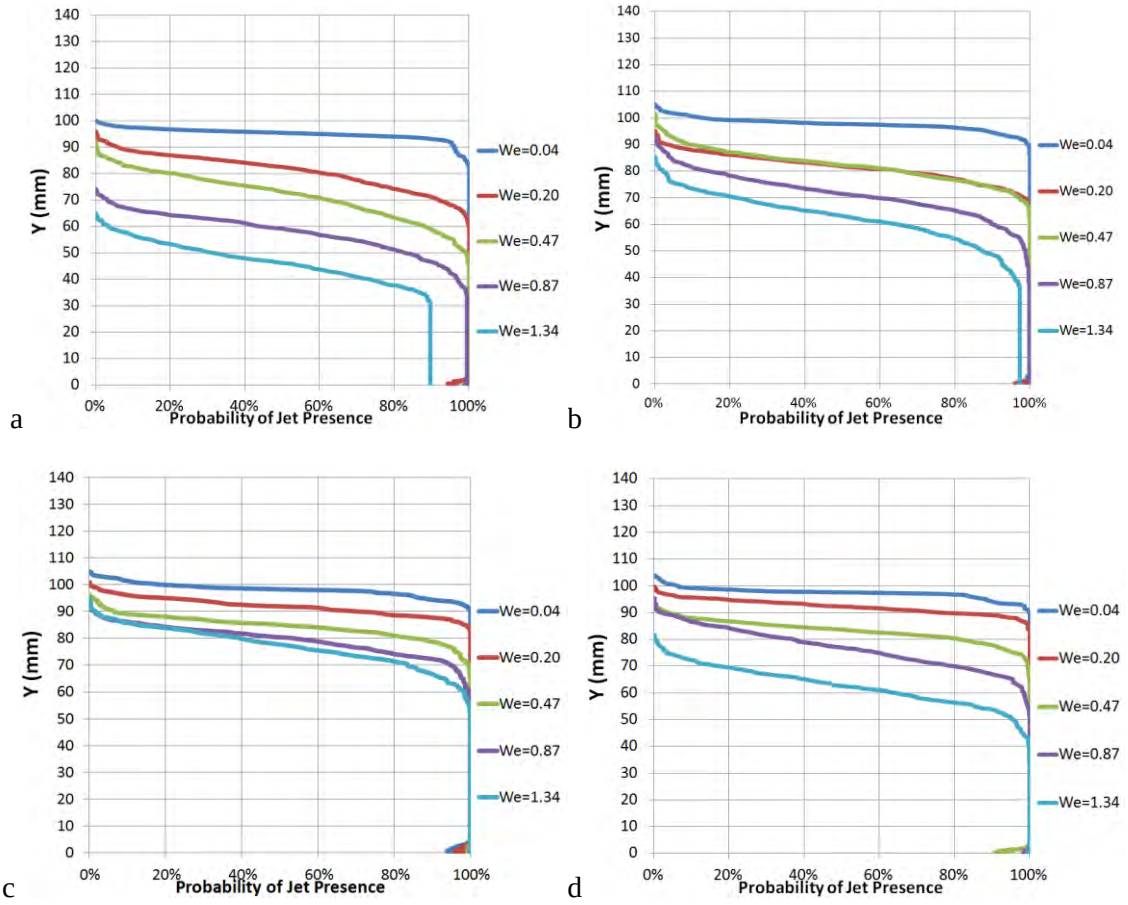

Figure 4.14: Probability of liquid jet presence downstream the jet for a) Re=1349, b) Re=2046, c) Re=2539, d) Re=2993 and We=0.04, 0.20, 0.47, 0.87, 1.34

5. Conclusions

5.1 Summary and Conclusion

An investigation was conducted on the injection of a liquid jet into a gas cross flow. The investigation was conducted in the domain of the Reynolds number, the aerodynamic Weber number, and the air to liquid momentum ratio which spanned the range of Re=1349-2993, We=0.04–1.34 and $q=1*10^{-4}$–$161*10^{-4}$. The liquid jet was visualised using shadowgraphy. It was found that:

1. For constant liquid Reynolds number, as the aerodynamic Weber number is increased the liquid jet deflection increases, the liquid jet penetration increases in the stream-wise direction and the penetration in the cross-stream direction decreases.
2. For Re=1349 and We=1.34 the liquid jet fluctuations are too great to obtain a mean profile as the liquid jet disintegrates quickly.
3. For constant We number, when the liquid Reynolds number is increased, the liquid jet trajectory deflection decreases due to the decrease of the air to liquid momentum flux ratio.
4. Fitting of the mean trajectories to power law functions showed that the law curve fits well to the experimental trajectories. The mean absolute error between the measured and the modelled trajectory was generally below 1mm for penetration lengths exceeding 50mm.
5. The fluctuation of the liquid jet, as quantified by the standard deviation of the liquid jet in the stream-wise direction, showed a negative correlation with the Re number and a positive correlation with the We number.
6. The probability of penetration of the liquid jet into the cross stream direction increases with the Re number and decreases with the We number.

5.2 Suggestion for Future Work

Although the experimental process has been carried out successfully and the experimental measurements on the liquid jet in cross flow were good, further future work can be done to investigate different objectives than the present study.

1. The investigation can be expanded to higher liquid jet and gas cross-flow velocities, in order to match the Reynolds and Weber numbers found in engine conditions.

2. Another possibility could be the investigation of different liquids with dissimilar physical properties such as viscosity and examine how the liquid jets develop for the same cross-flow conditions. A suggested liquid is glycerine which has high viscosity and can be used to similate the viscosity of kerose under sub zero temperature injection.
3. An issue that should be examn further is the outlier results for the cases with the highest aerodynamic Weber. Improvement must be done in the image processing algorithm in order to reduce the noise of the identified structures of the liquid jet.
4. Additionally an investigation should be carried out on spray atomization in gaseous cross-flow where the liquid jet is fully disintigrated into ligaments and various of droplets by utilising the external air supply of the atomiser.

6. References

Ain, H. ul. (2012). Simulation of Instabilities occurring in Liquid Jets. *Friedrich Alexander University*, 1–56. https://doi.org/10.1073/pnas.95.24.14147

Arai, M., Shimizu, M. & Hiroyasu, H. (1991). Similarity between the breakup lengths of a high speed liquid jet in atmospheric and pressurized conditions.

Atay I., Gordon, L., and Richard, T. (1987). Fluid flow and gas absorption in an ejector venturi scrubber, 198–203.

Becker, J. and Hassa, C. (1999). Breakup and atomization of a kerosene jet in crossflow of air at elevated pressure.

Chen, T.H., Smith, C.R., Schommer, D.G., and Nejad, A. S. (1993). Multi-zone behavior of transverse liquid jet in high-speed flow.

Dumouchel, C. (2008). On the experimental investigation on primary atomization of liquid streams, 371–422. https://doi.org/10.1007/s00348-008-0526-0

Faeth, G. M. (1999). Liquid Atomization in Multiphase Flows. In *30th AIAA Fluid Dynamics Conference* (pp. 1–19). Norfolk, VA, USA.

Hadjiyiannis, C. (2014). *Investigation of break-up process of liquids and downstream spray characteristics in air-blast atomisers*. Imperial College London.

Haenlein, A. (1932a). Disintegration of a liquid jet. *NACA TM 659*.

Haenlein, A. (1932b). Disintegration of a liquid jet. *NACA TN 659*.

Kadocsa, A. (2007). *Modeling of Spray Formation in Diesel Engines*.

Kekesi, T. (2017). *Scenarios of drop deformation and breakup in sprays*.

Lefebvre. (1989). Atomization and sprays.

Lefebvre, A. H., & McDonell, V. G. (2017). *Atomization and Sprays* (second). CRC Press.

Mazallon, J., Dai, Z., Faeth, G. M. (1999). Primary breakup of nonturbulent round liquid jets in gas crossflows, 291– 311.

N. Ashgriz. (2011). *Handbook of Atomization and Sprays Theory and Applications*.

Ohnesorge, W. (1936). Formation of drops by nozzles and the breakup of liquid jets/Die Bildung von Tropfen an Düsen und die Auflösung flüssiger Strahlen. *ZAMM - Journal of Applied Mathematics and Mechanics / Zeitschrift Für Angewandte Mathematik Und Mechanik*, *16*, 355–358. https://doi.org/10.1002/zamm.19360160611

OHNESORGE, W. (1936). Formation of drops by nozzles and the breakup of liquid jets. *Journal of Applied Mathematics and Mechanics 16*, 355–358.

Rayleigh, L. (1878a). On the instability of jets. *Proceedings of the London Mathematical Society*, *10*, 4–13. https://doi.org/10.1112/plms/s1-10.1.4

Rayleigh, L. (1878b). On the instability of jets, *Vol. 10*, 4–13.

Reitz, R. D. (1987). Modeling Atomization Processes in High-Pressure Vaporizing Sprays Y-l, *3*, 309–337.

Ross, S. M. (2009). Introduction to Probability and Statistics for Engineers and Scientists. *Fourth Ed*.

Sallam, K. A., Aalburg, C., & Faeth, G. M. (2004). Breakup of Round Nonturbulent Liquid Jets in Gaseous Crossflow. *AIAA Journal*, *42*(12), 2529–2540. https://doi.org/10.2514/1.3749

Savart. (1833). Mémoire sur la constitution des veines liquides lancées par des orifices circulaires en mince paroi. *Ann. Chim. Phys*, *53*(337).

Sina Ghods. (2013). *Detailed Numerical Simulation of Liquid Jet In Crossflow Atomization with High Density Ratios*.

Sinha, A., Surya Prakash, R., Madan Mohan, A., & Ravikrishna, R. V. (2015). Airblast spray in crossflow - structure, trajectory and droplet sizing. *International Journal of Multiphase Flow*, *72*, 97–111. https://doi.org/10.1016/j.ijmultiphaseflow.2015.02.008

Sou, A., Hosokawa, S., & Tomiyama, A. (2007). Effects of cavitation in a nozzle on liquid jet atomization. *International Journal of Heat and Mass Transfer*, *50*(17–18), 3575–3582. https://doi.org/10.1016/j.ijheatmasstransfer.2006.12.033

Sutradhar, S. C. (2012). *Validation of Atomization and Evaporation Models for Fuel Spray in Constant-Volume Experiments Under Non-Reacting Conditions*.

Weber. (1931). Zum Zerfall eines Flussigkeitstrahles.

Wierzba. (1993). Deformation and Breakup of Liquid Drops in a Gas Stream at Nearly Critical Weber Numbers, *vol 9*.

Wu, & P.-K., Kirkendall, K.A., Fuller, R.F., Nejad, A. . (1997). Breakup processes of liquid jets in subsonic crossflows.